Variation in platinum group mineral and base metal sulfide assemblages in the Lower Group chromitites of the western Bushveld Complex, South Africa

Bachmann, K.; Osbahr, I.; Tolosana-Delgado, R.; Chetty, D.; Gutzmer, J.;

Originally published:

September 2018

The Canadian Mineralogist 56(2018)5, 723-743

DOI: https://doi.org/10.3749/canmin.1700094

Variation in platinum group mineral and base metal sulfide assemblages in the Lower Group chromitites of the western Bushveld Complex, South Africa

Running Title: PGM and BMS in the LG chromitites, western Bushveld

Kai Bachmann[1,2]*, Inga Osbahr[1,3], Raimon Tolosana-Delgado[1], Deshenthree Chetty[4], Jens Gutzmer [1,2]

[1]Helmholtz-Zentrum Dresden-Rossendorf, Helmholtz Institute Freiberg for Resource Technology, Bautzner Landstraße 400, 01328 Dresden, Germany

[2]Department of Mineralogy, TU Bergakademie Freiberg, Brennhausgasse 14, D-09596 Freiberg/Sachsen, Germany

[3]Deutsche Rohstoffagentur (DERA) at the Bundesanstalt für Geowissenschaften und Rohstoffe, Wilhelmstrasse 25-30, 13593 Berlin-Spandau, Germany

[4]Mineralogy Division, Mintek, Malibongwe Drive, 2125 Randburg, South Africa

*Tel: +49 351 260 4426

Fax: +49 351 260 4440

k.bachmann@hzdr.de

Abstract

The Lower Group chromitites of the Bushveld Igneous Complex are mined for chromite as a primary product. The recovery of platinum group elements and base metals (Ni, Cu) as by-products has the potential to add value to the chromite resources. This study focuses on the LG-6 and LG-6A chromitite seams at the Thaba mine located on the western limb of the Bushveld Complex. Platinum group minerals and base-metal sulfides are studied by mineral liberation analysis and electron microprobe analysis to define distinct assemblages and to evaluate the potential for beneficiation. Based on the results two distinct major mineral assemblages are defined: The first assemblage is rich in platinum group element-sulfides, along with variable proportions of malanite/cuprorhodsite and alloys of Fe and Sn. The associated base metal sulfides are dominated by chalcopyrite and pentlandite, along with pyrite and subordinate millerite/violarite. Associated silicates are mainly primary magmatic orthopyroxene and plagioclase. The second assemblage is rich in platinum group element-sulfarsenides and -arsenides as well as -antimonides and -bismuthides, which are associated with a base metal sulfide assemblage dominated by pentlandite and Co-rich pentlandite. The assemblage is also marked by an abundance of alteration minerals, such as talc, serpentine and/or carbonates, which are closely associated with the platinum group minerals. Statistical evaluation reveals that these two mineral assemblages cannot be attributed to their derivation from different chromitite seams, but document the effects of pervasive hydrothermal alteration. Alteration evidently had similar effects on the different chromitite seams. The occurrence and distribution of the two characteristic assemblages has important implications for beneficiation. Assemblages rich in platinum group element-sulfides associated with base metal sulfides respond well to flotation, different to alteration assemblages rich in arsenides, antimonides and bismuthides. The nature of the gangue minerals will also impact platinum group mineral recovery as high phyllosilicate abundances, such as that encountered in the alteration assemblage may cause problems during flotation and lead to poor recoveries.

Keywords: SEM-based image analysis, ANOVA, Cluster Analysis, PGM, Thaba Mine, Bushveld Complex, EPMA

Introduction

The Bushveld Igneous Complex in South Africa is the world's largest layered mafic-ultramafic intrusion. The Rustenburg Layered Suite (RLS), comprising the most significant portion of the Bushveld Complex, consists of 7.5 to 9 km thick mafic and ultramafic cumulate rocks, covering an area of approximately 65,000 km^2. The RLS was emplaced approximately 2,056 Ma ago (2,055.91±0.26; Zeh et al. 2015) and can be subdivided into the Marginal, Lower, Critical, Main, and Upper Zones (Hall 1932, Figure 1A).

The RLS hosts 21 chromitite seams (*e.g.*, Fourie 1959; Naldrett et al. 2012; 16 are shown in Figure 1B). According to their stratigraphic position these are subdivided into lower, middle and upper group chromitites. The Lower Group (LG) and Middle Group (MG) chromitites are extensively mined for chromite as a primary product (*e.g.*, the mines Doornbosch, Winterveld, Lannex, Tweefontein and Dwarsrivier; DERA 2013). The uppermost of the chromitite seams (UG-2), in contrast, is exploited for platinum-group elements (PGE) as the primary economic product as it reaches PGE concentrations up to 10 ppm Σ[PGE+Au] (Von Gruenewaldt et al. 1986; Lee 1996; Cawthorn 2011). Base metals and chromite are recovered from the UG-2 as by-products. Whilst all other chromitite seams do also contain elevated PGE concentrations, these range only from 0.5 to 3 ppm (Wagner 1929; Von Gruenewaldt 1977; Von Gruenewaldt et al. 1986; Lee and Parry 1988; Cawthorn 1999; Barnes and Maier 2002; Naldrett et al. 2009a; Naldrett et al. 2012). Additionally, the chromitites display a progressive increase in PPGE (Pt+Pd+Rh) from the LG to the UG chromitites, whereas the content of IPGE (Os+Ir+Ru) remains broadly constant or increases only slightly (Naldrett and von Gruenewaldt 1989; Scoon and Teigler 1994; Naldrett et al. 2009b). This trend coincides with decreasing Cr/Fe ratios of the chromitites and results in a focus of mining the MG and LG seams for chromite (DERA 2013). The exploitation of PGE in the MG and LG seams is currently regarded as sub-economic (Oberthür et al., 2016).

Published knowledge on the mineralogy and deportment of PGE and base metals in the LG chromitite seams is scant (Teigler and Eales 1993; Scoon and Teigler 1994; Naldrett et al. 2009b, 2012; Junge et al. 2016; Oberthür et al. 2016) and beside the investigation of Maier and Barnes (Maier and Barnes 1999, and references therein) at Union Section, only scarce information is available in particular for the northern part of the western limb of the Bushveld Complex. The UG-2, in contrast, has been investigated in great detail (*e.g.*, McLaren and De Villiers 1982; Gain 1985; Hiemstra 1985, 1986; Maier and Barnes 2008; Cawthorn 2011; Junge et al. 2014, 2015; Osbahr et al. 2014). Junge et al (2016) and Oberthür et al. (2016) emphasized the similarity of PGM of the LG-6 with the UG-2 chromitite. However, with samples derived for these studies from reworked chromite dumps, they may yield representative results but lack any geological context. Given the scarcity of published data, it is not surprising that the mechanism of PGE enrichment in chromitite seams remains a subject of debate. Controversial aspects include the sulfide-poor nature of the RLS (S contents commonly < 100 ppm; Scoon and Teigler 1994), and the presence of discrete PGM containing almost the entire budget of PGE (*e.g.*, Hiemstra 1986).

Studies on the beneficiation characteristics of PGM and base metal sulfides (BMS) in Bushveld chromitite seams other than the UG-2 are very scant – as most published contributions focus on those resources currently exploited (UG-2, Platreef and Merensky Reef) (*e.g.*, Penberthy et al. 2000; Bulatovic 2003; Shackleton et al. 2007a,b; Brough et al. 2010; Becker et al. 2008; Chetty et al. 2009, Voordouw et al. 2010, Bushell 2012, Smith et al. 2013, Becker et al. 2014). These studies confirm that characteristics such as quantitative mineralogy, deportment, mineral association and grain sizes play a major role in PGM beneficiation. The type of PGM species, their liberation and association are particularly relevant for floatability (*e.g.*, Penberthy et al. 2000; Chetty et al 2009) as well as the association of PGM with BMS (Xiao and Laplante, 2004). PGM association with gangue minerals displays a separate set of challenges for flotation processes (*e.g.*, Chetty et al. 2009). Furthermore, Penberthy et al. (2000) reported that the grain size of PGM also affects floatability, with very fine (*i.e.* <3 µm) PGM considered as slow floaters.

Despite these constraints a possible recovery of base metals and PGE as by-product during exploitation of chromite would certainly add value and increase resource efficiency of chromite mining ventures. A successful example in this regard is Sylvania Platinum Ltd., reworking chromite dumps of the LG-6 and MG-1/2 chromitites from the eastern and western Bushveld Complex and producing saleable concentrates of both PGE and chromite (Junge et al. 2016; Oberthür et al. 2016).

This study focuses on the LG-6 and LG-6A chromitite seams located at the Thaba mine, a chromite mine situated on the western limb of the Bushveld Complex (Figure 1A) that is operated by Cronimet Chrome Mining SA (Pty) Ltd., a subsidiary of the Cronimet Mining Group. The proven reserves at Thaba total 23.6 Mt of chromite ore at 43.6 wt% Cr_2O_3 resulting in ca. 10 Mt contained Cr_2O_3 (DERA 2013). Mining started in 2011 and the life of mine is estimated at 26 years (DERA 2013). The mine exploits the LG-6/LG-6A as well as the MG-1 to MG-4A chromitite seams. Any PGE recovery needs to follow, or be integrated with, the recovery of chromite as the primary product.

In the present study, samples were obtained from three drill core intersections of the LG-6 and LG-6A chromitites at Thaba mine. The aims of the study are:

(i) to characterize the PGM and base metal sulfide and Fe-sulfide (BMS) assemblages by *in-situ* analysis of polished thin section surfaces of LG-6/LG-6A chromitite using scanning electron microscopy–energy dispersive X-ray spectrometry (SEM-EDS)-based image analysis techniques, complemented by electron microprobe analysis (EPMA),

(ii) to provide data on the composition of major silicate minerals and chromite,

(iii) to relate observed systematic changes in mineralogy and mineral association to geological processes,

(iv) to discuss the obtained data with respect to published work and to assess implications for the beneficiation of the chromitite ores.

The results are used to constrain the nature, distribution and origin of PGM and BMS in the chromitites of the RLS. Furthermore, our study provides important constraints for eventual beneficiation, as we consider not only qualitative mineralogy and mineral assemblage, but also quantify relevant attributes such as mineralogy, mineral grain sizes and mineral association for PGM and BMS. The *in-situ* methodology approach used in this study is preferred compared to the more widely employed method of studying grain mounts of PGM concentrates (*e.g.*, Junge et al. 2016; Oberthür et al. 2016) as it eliminates limitations to produce statistically significant results, for parameters such as mineral association, as shown elsewhere (*e.g.* Penberthy et al. 2000; Voordouw et al. 2010; Viljoen et al. 2012; Smith et al. 2013).

Analytical Methods

Access to diamond drill core intersections of LG-6 and LG-6A chromitite seams at Thaba mine was granted by Cronimet Mining Group. Drill cores were logged to document the lithological architecture of each intersection. Quarter drill cores were sampled with the goal to sample "pristine ores" below the extent of present-day weathering, *i.e.* to depth in excess of 50m below the present-day land surface, across the mine lease area. This approach was successful as none of the studied samples revealed any evidence of supergene oxidation of BMS. Six different drill core locations were selected for this study (Table 1), three of them for sampling of LG-6 (EL28, ZK149, ZK144) and three for LG-6A (EL32, ZK136, SC42). Deflections were considered wherever available. Samples from deflections are always demarcated by adding a D to the drill hole location name (Table 1). Chemical assay data for some of the selected drill cores were made available by Cronimet Mining Group. Available assay data refer always to entire chromitite seams; no assay data were available for drill cores ZK144, EL32D, and ZK136D.

The general sampling approach follows that of Voordouw et al. (2010). To investigate, if the LG-6 is bottom- or top-loaded with respect to PGM and BMS, each drill core intersection was divided into five distinct sectors: sector 1 covers the bottom 10%, sector 3 the mid 40% and sector 5 the top 10%

of the seam (sector 2 and 4 are each 20 %). Each sector was sampled randomly to prepare an individual polished thin section for study.. A similar approach was applied to the sampling of the LG-6A, but samples of sector 1 and 5 were set onto the contact between host rock and chromitite wherever this was possible. This resulted in a higher overall silicate proportion in the modal mineralogy than for the LG6 samples. Each section was cut vertical to stratigraphy.

Mineral Liberation Analysis (MLA)

Thirty polished thin sections of ca. 150 µm in thickness were prepared at the Helmholtz Institute Freiberg for Resource Technology (HIF). Each of these sections was analyzed twice by MLA on two polished surfaces well-separated by re-grinding and re-polishing. These two surfaces are referred to as surface A and surface B; all data and detailed investigations on the reproducibility of the MLA measurements can be found in the electronic supplementary material (Appendix A, B and C). The sections were analyzed twice to increase the number of PGM and BMS grains identified and to constrain intra-sample variation. Furthermore, two sample surfaces were analyzed as in-run duplicates to check for internal consistency of data acquisition.

The MLA instrument used in this study is located at the HIF and comprises a scanning electron microscope FEI Quanta 650F equipped with two Bruker Quantax X-Flash 5030 energy-dispersive X-ray spectrometers and the MLA 3.1.4 software suite for automated data acquisition. Consistent operating conditions were applied (Table 2). DataView (Fandrich et al. 2007) software was used for further processing of the data. All samples were analyzed using the sparse phase liberation (SPL_Lt) and the grain X-ray mapping (GXMAP) mode (Fandrich et al., 2007). Standard spectra were collected for all relevant minerals. Selected grains of silicates, BMS and PGM were then analyzed by electron microprobe (EPMA, see below). More detailed information about the functionality of a MLA and the joint offline processing of EPMA and MLA data can be found in Gu (2003) and Bachmann et al. (2017).

As shown by Voordouw et al. (2010), abundances of individual PGM, sulfides and silicates may differ from each other by an order of magnitude; the proportions of individual minerals are thus described within chemically similar groups rather than in absolute terms (*e.g.*, area%$^{\mathrm{PGM}}$ refers to the area% of individual PGM among all PGM).

Electron probe microanalysis (EPMA)

Electron probe microanalysis was performed with a JEOL JXA 8530F at the HIF equipped with a field emission electron gun and five wavelength dispersive spectrometers (WDS). Five different analyzer crystals TAP, PETJ, PETL, PETH, and LIFH on five spectrometers were utilized to measure chemical compositions of various base metal and iron sulfides (BMS) as well as PGM. Quantitative EPMA analyses were also performed on major silicates and chromite. Detailed information about the methodology and the entire data set is provided in the electronic supplementary (Appendix A and D).

The assignment of the analyzed elements to detector crystals and spectrometers as well as peak and background positions, dwell times and the lower limit of detection during PGM and BMS analyses are shown in Table 3. All quantitative analyses were performed with a focused beam at an accelerating voltage of 12 kV/ 20 kV and a beam current of 100 nA/ 30 nA. Analyses were corrected according to the measurement protocol of Osbahr et al. (2015), slightly modified by a time-resolved offline overlap correction and a step-wise overlap correction of multiple interferences. EPMA results were further used to generate mineral standard spectra with a known composition for MLA measurements.

Statistics

Statistical data evaluation and comparison of properties across the data set was obtained via ANalysis Of VAriance (ANOVA, *e.g.* Fahrmeir and Hammerle, 1984), which explains the variance of several target (predicted) variables by the influence of certain explanatory factors. In our case the modal mineralogy in respectively area%$^{\mathrm{PGM}}$, area%$^{\mathrm{BMS}}$, area%$^{\mathrm{Gangue}}$ (Gangue: alteration silicates, silicates, carbonates) are predicted variables. Other minerals occurring in trace quantities, such as monazite, zircon, etc, were not considered as they add no relevant information. Chromite was not considered because the chromite content is strongly dependent on the sampling location, *i.e.* massive chromitite, chromitite with silicate intercalations or chromitite – host rock contact. Explanatory factors considered were: The section surface (A/B), the relative stratigraphic position within a seam "intra seam" (top, top-middle, middle, bottom-middle and bottom), and either the seam (LG-6 vs. LG-6A) or the borehole (EL28D-LG-6, ZK149-LG-6, ZK144-LG-6, EL32D-LG-6A, ZK136D-LG-6A vs.SC42-LG-6A, "inter-core" effects). ANOVA allows to test in an organized manner, which of these variables exert a significant, systematic control on the area% composition of the mineral groups considered. This is achieved by F-tests targeting each explanatory variable, and checking the null hypothesis that the residual variability of a model including that target variable is the same as a model without it. If this would be the case, then the target variable would not reduce the uncertainty about the explained composition, and should be discarded. In practical terms, for those variables for which the F-test returned a significance level of $p < 0.05$, the null hypothesis is rejected, hence the target variable is accepted as having a significant influence on the composition. Significance levels considered are: 0-0.001 highly significant, 0.001-0.01 moderately significant, 0.01-0.05 significant, 0.05-1 not significant.

A cluster analysis for the mineral association of PGM and BMS was performed to support the separation into distinct ore types suitable for further treatment in a mineral beneficiation process. The R software environment (R Core Team 2016) with the additional packages "mclust" (Fraley and Raftery 2002) and "compositions" (van den Boogaart et al. 2014) were used for data analysis. The algorithm "mclust" requires a choice of the characteristics (orientation, size and shape) of the covariance matrix which are allowed to vary between groups: the analysis was done in "VVV"-mode, meaning that each cluster was allowed to have a totally different covariance matrix (Fraley et al. 2012). All modal mineralogy subcompositions were treated with the statistical framework of compositional data analysis (Aitchison, 1986; Tolosana-Delgado, 2012), to avoid the effects of spurious correlation occurring in such closed subcompositions (Chayes, 1960). To get rid of these effects, the solution chosen here is to work with ratios or log-ratios between components.

Results

Results are presented in three sections. The first provides a brief description of the lithological architecture and qualitative petrographic appearance of the LG-6 and LG-6A chromitite seams sampled. The following section reports the results of EMP analysis, *e.g.* the mineral chemistry of PGM and BMS. This data is complemented by analyses of silicates and chromite provided in the electronic supplement (Appendix A). Finally, MLA results are evaluated in terms of modal mineralogy (sub-compositions PGM/BMS/Gangue as defined above) and mineral association (PGM/BMS).

Lithology and Mineralogy

This section provides largely qualitative descriptions of the studied chromitite seams – and their mineralogy. Quantitative mineralogical data is provided later in this contribution. The LG-6 and LG-6A chromitite seams at Thaba mine are well developed as massive, single seams that are usually hosted by pyroxenite. The LG-6 seam as the primary mining target averages 0.85 m in thickness, varying between 0.34 m and 1.37 m; the Cr_2O_3 content averages 43.1 % and the Cr:Fe ratio is 1.58. The LG-6A occurs stratigraphically approximately 6 m above the LG-6 seam and averages at 0.23 m in thickness, containing on average 41.2 % Cr_2O_3 with a Cr:Fe ratio of 1.48. Locally, cm-thin chromitite stringers (such as in sample EL028-LG-6) or pegmatoidal pyroxenite (ZK136-LG-6A and EL32D-LG-6A) occur in the pyroxenite host rock. Footwall (0.2 m) and hanging wall (1 m) of EL32D-LG-6A consist of serpentinite (altered pyroxenite) while some of the pyroxenite in intersection ZK149-LG-6 is also strongly serpentinized.

All chromitite samples selected for this study are best described as massive chromitites that are comprised mostly of chromite, orthopyroxene and plagioclase. Thin intercalations of silicate rocks as well as up to a few cm long silicate oikocrysts are locally common in these massive chromitites.

Chromite grains are subspherical in shape, with average diameters of < 0.5 mm (max. ~1 mm), and smooth grain margins. Chromite grains may host inclusions of silicates, sulfides and Fe-Ti oxides. Subvertical veinlets are common, containing variable amounts of mica, amphibole and minor carbonates. Especially in sample EL32D-LG-6A, chromite grains appear fractured and are cemented by a younger generation of chromite.

The silicate minerals have been subdivided into two assemblages. The first assemblage includes silicates regarded as orthomagmatic in origin (called silicates group), the other assemblage includes all (hydrous) silicates that are considered to have formed by post-magmatic hydrothermal alteration (called alteration silicates group). The silicates group is dominated by pyroxene (more orthopyroxene than clinopyroxene), followed by feldspar, and traces of olivine, while quartz is almost absent. Mica is present in very minor abundances and is biotitic in composition. Feldspar compositions are dominated by plagioclase, alkali feldspar occurs only in trace amounts. In intersections ZK149-LG-6 and EL32D-LG-6A, feldspar is entirely absent.

The alteration silicates group is dominated by amphibole, chlorite (mainly clinochlor) and talc, while only minor serpentine is present. Carbonate minerals (mainly of dolomitic compositions) were also identified as part of the hydrothermal alteration assemblage and occur only in very minor amounts. A notable exception is the occurrence of dolomite in chromitite seam LG-6A of drill core EL32D.

PGM and BMS occur in all samples in trace amounts. PGM are observed as monomineralic grains, which may show internal zonation, but also as aggregates of variable complexity (for representative examples see Figures 2B-H). Equivalent circle diameters (ECDs, value of the diameter of a circle having the same area as the measured grain/particle; *e.g.*, Fisher et al. 1987) of PGM grains/ aggregates typically range between <1 and 20 µm, ECDs of up to 35 µm are scant. Average ECDs are consistently between 4 µm and 5 µm. PGM are often locked or attached to BMS but also occur enclosed in or interstitial to chromite, silicates and alteration silicates. PGM enclosed within chromite grains consist mainly – but not exclusively - of laurite (Figure 2G). Members of the laurite [RuS_2] -

erlichmannite [OsS_2] series are also the main carriers of IPGE (iridium-subgroup; Ir, Ru, Os). Minerals belonging to the cooperite-braggite-vysotskite [PtS – (Pt,Pd)S – PdS] series and members of the thiospinel solid solution series malanite [$CuPt_2S_4$]-cuprorhodsite [$CuRh_2S_4$] are major carriers of the PPGE (platinum subgroup; Pt, Pd, Rh). Sperrylite [$PtAs_2$], PGE-antimonides, -bismuthides and -bismuthotellurides such as geversite [$PtSb_2$], and stibiopalladinite [$Pd_{5+x}Sb_{2+x}$] with minor sudburyite [PdSb], insizwaite [$PtBi_2$], and traces of genkinite [$(Pt,Pd)_4Sb_3$] and moncheite [$(Pt,Pd)(Te,Bi)_2$] are of lesser abundance as are PGE-alloys including rustenburgite [Pt_3Sn] and tetraferroplatinum [PtFe]. Traces of native platinum [Pt] were also identified. Sulfarsenides (platarsite [PtAsS], hollingworthite [RhAsS] and irarsite [IrAsS]) with variable compositions contribute significantly to the overall PGE budget in some samples.

BMS usually occur as aggregates up to 300 µm in diameter or as single grains (<100 µm), interstitial to chromite or enclosed in silicates. Smaller (up to 100 µm) aggregates of BMS were found as inclusions in chromite. Importantly, pyrrhotite is almost absent. In general, BMS are dominated by pentlandite [$(Ni,Fe)_9S_8$], which in some cases contains minor concentrations of Co. Other important Ni-sulfides are millerite [NiS] and violarite [$Fe^{2+}Ni_2^{3+}S_4$]. Violarite often rims and replaces pentlandite (Figure 2A, D). Some examples of millerite and violarite do also contain minor amounts of Co. Chalcopyrite and pyrite only occur in some samples in significant amounts – relative to the other BMS. Galena, stibnite and sphalerite were detected only in negligible abundance – they are not considered further.

Geochemistry and Mineral Chemistry

5PGE+Au (Pt,Pd,Rh,Ir,Ru,Au) contents are around 1 ppm for LG-6 samples and 1.5 ppm for the LG-6A, with a Pt/Pd ratio around 2.2 and 4 and Pt/Ru ratios around 0.9 for intersections ZK144-LG-6 and ZK149-LG-6, respectively. In general, the total sulfur content ranges between 100 – 200 ppm (<250 ppm), except intersection ZK144-LG-6, which contains only around 70 ppm. Arsenic contents are usually below the detection limit (<0.5 ppm), except in a few samples of ZK149-LG-6 (up to 9 ppm). Detailed data is provided with the electronic supplement (Appendix A and E).

Mineral chemistry data was obtained for all relevant rock-forming mineral groups, except chlorite and mica. Pyroxenes, amphiboles, serpentine and talc, as well as chromite compositions are well discriminated by their mineral chemistry. Two different types of pyroxenes were detected, an orthopyroxene (hereafter referred to as enstatite with Mg/ (Mg+Fe^{2+}) ratios ranging from 0.82-0.84) and a clinopyroxene with augitic to diopsidic composition (hereafter referred to as diopside). Amphiboles can be best described as magnesio-hornblende. Feldspars yield plagioclase compositions (Median = An_{66}). In general, chromite displays Mg/(Mg+Fe^{2+}) cation ratios around 0.42 (sample EL32D-LG-6A around 0.33), while Cr/(Cr+Al) cation ratios plot at 0.73 (EL32D-LG-6A: ~0.64). Detailed data and methodology are provided in the electronic supplement (Appendix A and D).

The composition of PGM and BMS is collated in Tables 4 and 5. Mineral chemistry data were used to provide proper identification of PGM in MLA data sets – and to characterize BMS in greater detail. Pentlandite displays rather variable compositions, especially regarding the concentration of Co. For the purpose of this study we refer to pentlandite containing > 2 wt% Co as Co-rich pentlandite. Pyrite analyses reveal Co and Ni contents up to 1.5 wt% and 3.5 wt%, respectively.

A notable number of pyrite, pentlandite, Co-rich pentlandite and violarite analyses as well as a few chalcopyrite analyses yielded measureable PGE concentrations. Pyrite, pentlandite and Co-rich pentlandite yield concentrations up to 2-3 wt% Rh, Pt, Ru and Ir, around 1 wt% Pd and up to 0.5 wt% Os. Chalcopyrite was found to contain PGE contents below 1 wt% and violarite up to 0.4 wt% Rh and 0.2 wt% Pd, respectively. Despite the fact that several previous studies have suggested that BMS can contain significant amounts of PGE (Osbahr et al. 2013; Osbahr et al. 2014; Junge et al. 2014), the concentrations reported in this study are unusually high. We tentatively consider the PGE as being localized as submicroscopic inclusions of discrete PGM in the BMS (see Figure 2H), occasionally hit by spot analyses during the EPMA measurements.

Quantitative Mineralogy and Microfabric Data

Quantitative mineralogical and microfabric data were obtained by MLA analysis. In order to facilitate comparison, the rock-forming minerals were grouped as follows (sorted by abundance): Chromite (Al-rich spinel, various chromite compositions), silicates (ortho- and clinopyroxene, feldspar, olivine, quartz, biotite), alteration silicates (amphiboles, chlorite, muscovite, serpentine, talc), carbonates (calcite, dolomite), others (*e.g.*, apatite, barite, monazite, rutile, titanite, zircon). For PGM and BMS compositional sub-groups were defined (Table 6). The relative abundance of these is expressed as area%^{PGM} and area%^{BMS} – this was done to ease comparison between different samples. The same was done for gangue mineral groups (alteration silicates, silicates, carbonates) – these are expressed as area%^{Gangue}.

The quantitative mineralogy of all sampled seams is given in Table 7. For this purpose, data obtained for all five samples collected from each seam was combined. Data for PGM and BMS for every thin section surface analyzed is provided in the electronic supplement (Appendix C). This investigation uses relative abundances of different PGM subgroups for classification. As illustrated in Figure 3A, minerals belonging to the $(Ru,Ir,Os)S_2$ subgroup are present in all samples, but comprise rather different proportions of the total PGM population (LG-6: 17 up to 59 total area%^{PGM}; LG-6A: 6 up to 64 total area%^{PGM}). In samples El28D-LG-6, ZK144-LG-6, ZK136D-LG-6A and SC42-LG-6A (Pt,Pd)S and $(Pt,Rh)_2CuS_4$ are common PPGE carriers subordinate only to alloys containing Fe and Sn; the latter range from 30 to 68 total area%^{PGM} in the LG-6 and from 33 to 65 total area%^{PGM} in the LG-6A seam. $(Pt,Rh)_2CuS_4$ is the dominant PPGE carrier in ZK144-LG-6. In contrast, the PGM assemblage in samples ZK149-LG-6 and EL32D-LG-6A is dominated by (PGE)As,AsS and (PGE)Sb,Bi, comprising 44 to 76 total area%^{PGM} in ZK149-LG-6 and 53 to 85 total area%^{PGM} in EL32D-LG-6A.

The BMS mineralogy is dominated by Co-rich pentlandite, chalcopyrite, millerite, violarite and pyrite as well as traces of pyrrhotite (Figure 3B). The sulfide proportions are highly variable. In samples ZK149-LG-6 and EL32D-LG-6A Co-rich pentlandite represents the majority of the BMS, while chalcopyrite, pyrite as well as minor millerite dominate sample ZK144. Samples EL28D, ZK136D and SC42 contain variable proportions of Co-rich pentlandite, chalcopyrite, pyrite/ (pyrrhotite), violarite and minor millerite.

Figure 3C displays the relative distribution of PGM and BMS of intersections of the LG-6 and LG-6A seams. While ZK144-LG-6 has a rather low BMS content and an assemblage dominated by chalcopyrite and minor millerite, both Co-rich pentlandite dominated intersections (ZK149-LG-6 and EL32D-LG-6A) display a high sulfide content (resulting in a distinctly higher sulfur content, *i.e.* sample ZK149-LG-6 compared to sample ZK144-LG-6). In contrast, the PGM contents are rather similar, with somewhat lower abundances in EL28D-LG-6 and EL32D-LG-6A and distinctly higher PGM contents in sample ZK144-LG-6.

Statistical Assessment

The application of statistical methods is needed to deal with the large number of samples and the multivariate datasets. This leads to the differentiation of three substantially distinct PGM-BMS assemblages:

(I) PGM-sulfides and alloys of Fe and Sn ± PGM-Cu-sulfides occur together with a BMS assemblage dominated by pentlandite + chalcopyrite + pyrite

(II) PGM-Cu-sulfides ± PGM-sulfides ± alloys of Fe and Sn; corresponding BMS are dominated by chalcopyrite + pyrite + millerite ± pentlandite

(III) PGM-sulfarsenides and PGM-arsenides occur together with PGM-antimonides and -bismuthides and scant tellurides; corresponding BMS are strongly dominated by pentlandite and Co-rich pentlandite ± chalcopyrite ± pyrite.

The following sections document the relative contribution of ANOVA and cluster analysis to this result.

ANOVA

An ANOVA was performed – followed by standard F-tests – to investigate the variability of the samples and to determine assemblages for classification according to the sub-compositions area%^{PGM}, area%^{BMS} and area%^{Gangue}. Detailed results can be found in the electronic supplementary material (Appendix A). Results suggest that the "nugget effect" (small scale variability) is negligible for all sub-compositions. The variance between samples of a different stratigraphic position within a sampled seam, *i.e.* if seams have systematically different mineral assemblages within their respective confines, should be noted – but remains small. Furthermore, there are no systematic changes in mineral abundances observed between the two chromitite seams LG-6 and LG-6A. Thus, the variability between certain drill cores explains up to 80 % of the total variability – depending on the selected sub-composition. A detailed investigation of the ANOVA model showed a strong negative correlation of PGE -sulfarsenides and PGE-antimonides, -bismuthides vs. PGE –sulfides, -Cu-sulfides and -alloys of Fe,Sn (for area%^{PGM}), along with (Co-rich) pentlandite against the other four BMS considered, namely chalcopyrite, millerite, pyrite and violarite (for area%^{BMS}). Furthermore, a negative correlation of PGE-Cu-sulfides vs. PGE –sulfides and –alloys of Fe,Sn along with chalcopyrite and millerite against pyrite and violarite was observed. The area%^{Gangue} assemblages are best classified by separating alteration silicates and silicates-rich from carbonate-rich drill cores, followed by a separation of alteration silicates from silicate-rich cores. While carbonate-rich samples are associated with PGM-BMS assemblage (III), silicate-rich samples dominate PGM-BMS assemblage (I). Significant amounts of alteration silicates may occur in samples belonging to PGM-BMS assemblages (II) and (III).

Cluster analysis

For a quantitative assessment of the variability of the mineral association a cluster analysis was performed according to the sub-compositions of PGM (without IPGE sulfides) and BMS. The results were linked to the mineral assemblages defined in the previous chapter (*ANOVA*). Detailed information can be found in the electronic supplementary material (Apendix A). Despite the very low total abundance of BMS (< 0.02 area% in all samples), PGM show a strong preferred association with BMS; they also show a close association with alteration silicates, occurring both in interstitial positions and as inclusion. PGM are only to a much lesser extent associated with silicates and chromite. PGM occur predominantly interstitial to chromite (with minor inclusions cf. Figure 2G). BMS show a very similar association to PGM.

Discussion

Appropriate statistical assessment of quantitative mineralogical data suggests the presence of three distinct PGM-BMS mineral assemblages in the LG-6 and LG-6A chromitite seams at Thaba mine. The LG-6 and LG-6A intersections show striking differences between different drill cores, resulting in variable PGM, BMS, and gangue mineral assemblages. The (para)-genetic relevance of the documented differences between these three assemblages is evaluated below. Finally, implications for recovery of PGM and BMS are briefly discussed.

General Aspects

The LG-6/LG-6A chromitites at Thaba mine share numerous similarities to lateral equivalents at other locations in the Bushveld Complex (e.g., Teigler and Eales 1993; Eales et al. 1993; Scoon and Teigler 1994; Naldrett et al. 2009b, 2012). Such similarities include:

(1) chromitites are developed as single seams hosted by pyroxenite,
(2) Cr:Fe ratio is 1.58 for the LG-6 and 1.48 for the LG-6A, respectively,
(3) orthopyroxenes yield Mg/(Mg+Fe^{2+}) ratios ranging from 0.82-0.84,
(4) intercumulus feldspar compositions within pyroxenites in the Lower Critical Zone are those of labradorite (Median = An_{66}),
(5) limited variation in chromite compositions,
(6) uniform PGE grades (5E + Au) around 1 ppm (LG-6) and 1.5 ppm (LG-6A),
(7) Pt/Ru ratios around 0.9, Pt/Pd ratios ranging from 2 to 4, and low S_{tot} ranging from 70 to 200 ppm.

We thus deem it likely that the observations made here can be transferred to other occurrences of LG chromitites within the Bushveld Complex.

Mineral assemblages

Different to previous investigations the present study offers quantitative mineralogical and microfabric data on *in-situ samples* (*i.e.* polished thin samples not modified by comminution or mineral separation) for PGM and BMS in the LG-6/LG-6A chromitites of the Bushveld Complex. The data provide unique insight into different PGM, BMS and rock-forming mineral assemblages and associations.

PGM assemblages are dominated by various Pt-Pd-Rh sulfides (cooperite-braggite and malanite-cuprorhodsite), laurite (the main carrier of the IPGE), sulfarsenides, sperrylite and Pt-Fe alloys; PGE-tellurides and PGE-bismuthotellurides are largely absent. These observations are rather similar to previous studies (*e.g.*, Junge et al 2016; Oberthür et al. 2016) carried out on mineral concentrates.

BMS occur only in very minor abundances. Pentlandite, Co-bearing pentlandite, chalcopyrite and pyrite dominate, whilst millerite is much less common. The virtual absence of pyrrhotite is noted. The BMS mineralogy is thus rather similar to that reported in previous studies for Bushveld chromitites (*e.g.*, Junge et al 2016; Oberthür et al. 2016).

Yet, despite these broad similarities, LG-6 and LG-6A chromitite intersections at Thaba mine reveal significant and systematic mineralogical variations that remained previously unnoticed. These mineralogical variations are observed in both the LG-6 and LG-6A – and can thus not be used to distinguish the two seams from one another. Rather, the differences need to be described as lateral variations independent of stratigraphic position.

Three different PGM-BMS assemblages were recognized (Figure 4):

(I) PGM-sulfides and alloys of Fe and Sn ± PGM-Cu-sulfides occur together with a BMS assemblage dominated by pentlandite + chalcopyrite + pyrite

(II) PGM-Cu-sulfides ± PGM-sulfides ± alloys of Fe and Sn; corresponding BMS are dominated by chalcopyrite + pyrite + millerite ± pentlandite

(III) PGM-sulfarsenides and PGM-arsenides occur together with PGE-antimonides, -bismuthides and scant -bismuthotellurides; corresponding BMS are strongly dominated by pentlandite and Co-rich pentlandite ± chalcopyrite ± pyrite

All three of these PGM-BMS mineral assemblages are interpreted to be the product of postmagmatic alteration, variably modifying an orthomagmatic assemblage.

Mineral assemblage (I) can be regarded as the most pristine assemblage, revealing a low alteration silicate to orthomagmatic silicate ratio. A relatively high BMS concentration and a variable PGM and BMS mineral association mark this assemblage. BMS display variable abundances of pentlandite, chalcopyrite, pyrite and minor violarite. PPGE carriers are PGE sulfides and PGE-Cu sulfides with variable proportions of PGE alloys of Fe and Sn. This is especially evident in intersection SC42-LG-6A, which contains significant amounts of violarite. While traces of millerite in EL28D-LG-6 and SC42-LG-6A as well as significant amounts of PGE alloys of Fe and Sn are consistent with beginning desulfidization, violarite is typically regarded as a product of late stage hydrothermal alteration of mixtures of iron-nickel sulfides (Dunn and Howes 1996; Tenailleau et al. 2006). Based on a statistical analysis a “typical” mineral association for PGM in assemblage (I) was defined. The dominating PGE-sulfides and -alloys of Fe and Sn are strongly associated to BMS and show only moderate affinity to silicates and alteration silicates (Figure 5).

Assemblage (II), best typified by sample ZK144-LG-6, is marked by the abundance of alteration silicates, although the alteration silicate to silicate ratio remains moderate. The total BMS content in assemblage (II) is rather low, as is the total sulfur content (~70 ppm). The BMS assemblage is dominated by chalcopyrite, pyrite and millerite. Minerals of the malanite-cuprorhodsite solution series are by far the most important carriers for PPGE in this assemblage.

BMS and PGM present in assemblage (II) suggest an origin by removal of Fe and S by either late magmatic fluids and/or by reaction of sulfide with chromite from an orthomagmatic assemblage (e.g. Naldrett et al 2012 and references therein). The high amounts of Ni-rich sulfides are explained through re-equilibration of Fe from magmatic sulfide liquid with chromite (Naldrett and Lehmann 1988).

The high abundance of hydrous silicates associated with assemblage (II) suggests that corrosive action of hydrothermal fluids further modified the BMS assemblage. That these fluids may play a major role to explain the loss of sulfides was shown, for example, for the UG-2 (Penberthy and Merkle 1999; Li et al. 2004, Voordouw et al., 2010). High malanite-group PGM concentrations in chromitite were recently documented by Oberthür et al. (2016). The latter authors proposed that part of the orthomagmatic chalcopyrite experienced a similar fate as the re-equilibrated Fe-sulfides and has reacted to some extent with cooperite/braggite to form malanite. Although the PGM mineralogy displays some similarities with assemblage (I), such as a similar PGM spectrum, the mineral association of these PGM is distinctly modified and strongly dominated by alteration silicates, minor silicates and lack of association with BMS.

Mineral assemblage (III) is best represented by intersections ZK149-LG-6 and EL32D-LG-6A and can be further linked to gangue mineral assemblages. According to the ANOVA results, the gangue mineral assemblage is closely related to assemblage (II). However, assemblage (III) generally displays a significantly higher ratio in alteration minerals to orthomagmatic silicates; in drill core ZK149-LG-6 this is due to an abundance of alteration silicates, whereas in drill core EL32D-LG-6A carbonates are particularly widespread. Host rocks of these two intersections display strong serpentinization and thus provide further evidence for pervasive hydrothermal alteration. Furthermore, chromite analyses display somewhat higher $Mg/(Mg+Fe^{2+})$ and $Cr/(Cr+Al)$ cation ratios (in sample EL32D-LG-6A). A model including alteration by As-bearing fluids is favored over crystallization directly from As-bearing melt as proposed by, e.g., Gervilla et al. (1996). Reasons for this interpretation include: (1) Investigated samples have very low As contents and contain no other arsenides, such as nickeline, etc., which would be expected in As-bearing melts. (2) PGE (sulf-)-arsenide-rich drill core intersections display other prominent alteration features, as described above. (3) PGE arsenide-rich assemblages of secondary origin are widely reported for the Bushveld Complex (Peyerl 1982; Kinloch 1982, Voordouw et al 2010). These arguments also support a secondary origin for PGE-antimonides and –bismuthides. The PGE-(sulf)-arsenides, -antimonides and -bismuthides occur closely associated with alteration silicates, carbonates or are interstitial to chromite. They show only a moderate affinity to BMS and are almost absent as inclusions in chromite (Figure 5). Beside the carbonate-dominated samples, the statistical assessment yielded similar results for the PGM mineral association in assemblage (III) and assemblage (II), due to the strong affinity to alteration silicates. Nevertheless, the low PGM affinity to silicates but higher affinity interstitial to chromite and to BMS, mainly pentlandite, points to different processes responsible for the modification of the original orthomagmatic mineral assemblage.

Laurite-group minerals, as the main IPGE carrier, deserve specific mention. They behave very different to other PGM, and show stable proportions over all drill core intersections. According to the statistical analysis laurite-group minerals remain unaffected by alteration processes. The same is true for pyrite and pyrrhotite. Even though these two Fe-sulfides were reliably separated from assemblage (III) in the ANOVA model, a further preferential association to assemblages (I) or (II) was not possible to elucidate. This might be caused by the variable appearance of pyrite, as mineral of primary (cf. Figure 2C) or possibly secondary origin (cf. Figure 2A, D), for example by replacing pyrrhotite or as a by-product of the violarite alteration of pentlandite.

Implications for beneficiation

Given the fact that PGM and BMS were investigated *in-situ* in this study, the following relevant parameters may be extracted and quantified from the data set for the potential recovery of PGM and BMS: 1. Mineral species; 2. Mineral association; 3. Grain size distribution and 4. Gangue mineralogy (*e.g.* Penberthy et al. 2000; Chetty et al. 2009). All these parameters are known to have a significant impact on PGM recovery by flotation (*e.g.* Becker et al. 2013; Ndlovu et al. 2014).

Table 8 summarizes all relevant parameters of the three noted assemblages for mineral beneficiation; similarities and differences between these assemblages are highlighted. Studies on the floatability of different PGM species in the UG-2 chromitite (*e.g.* Penberthy et al. 2000; Chetty et al. 2009) suggest a higher floatability of sulfide-rich PGM assemblages compared to sulfarsenide-rich assemblages. Flotation performance is also influenced by BMS and gangue mineralogy, as well as the textural relations between PGM and associated minerals.

Relatively high recoveries may thus be expected for the BMS-rich assemblage (I), since the PGM assemblage is not only sulfide-rich, but typically intergrown with a BMS assemblage marked by an abundance of fast-floating chalcopyrite (Penberthy et al. 2000; Smith et al. 2013). In contrast, the BMS content of assemblage (II) is significantly lower and PGM show rather little association to the contained BMS. Therefore, recoveries of PGM may be expected to be somewhat lower, despite the presence of PGM sulfides and chalcopyrite. Assemblage (III) can be expected to yield even lower recoveries. This is due to the dominance of slow-floating sulfarsenides and a close association of PGM with alteration silicates, chromite and carbonates – minerals that either do not float (chromite/carbonate) or that need to be depressed in the given flotation process (*e.g.*, talc). The high content of phyllosilicates in the alteration silicate association of assemblage (III) may be expected to have rheological impacts in flotation, leading to even lower recoveries, as discussed by *e.g.*, Becker et al. (2013) and Ndlovu et al. (2014).

In addition to the mineralogy of the three assemblages, the grain sizes of PGM and BMS will play an important role in defining recoveries during flotation. The average grain size of 4-5 µm ECD for the PGM and up to 300 µm ECD for BMS in all samples studied – irrespective of the actual assemblage. This suggests that PGM and BMS should be amenable to flotation, if fully liberated and not reduced further in size during comminution. PGM and BMS particle sizes <3 µm are generally considered to have poor flotation characteristics (Chetty et al. 2009). Nevertheless, to achieve sufficient liberation of the majority of the minute PGM grains will likely require fine milling – beyond the typical flotation feed of 45 – 80 % passing 75 µm typically used. However, the effects of ultrafine milling on liberation characteristics of PGM and BMS mineral grains and grain aggregates are beyond the purpose of this contribution. If PGM are associated with BMS – either because of intergrowth or because of the presence of minute inclusions of PGM – the grain sizes of PGM may in fact not be relevant for flotation - but rather the aggregate sizes and liberation of the BMS. These aggregates are typically larger than 30 µm, often up to a few 100 µm which will easily float and further improve PGE recovery.

Conclusion

Based on a combination of mineralogical and micro-analytical data, complemented by a tailored statistical assessment, our study delivers the first systematic evaluation of PGM and BMS assemblages in the LG's of the Bushveld Complex. According to our assessment, no truly unaltered orthomagmatic mineral assemblage is preserved at the site of study – the LG-6 and LG-6A chromite seams exploited at Thaba mine of the northernmost part of the western limb of the Bushveld Complex. Alteration is documented by changes to the PGM, BMS and gangue mineralogy, while chromite remains almost unaffected. Alteration assemblages are similar in both of the two studied LG seams. It was further demonstrated that lateral variation between different drill cores dominates over vertical variation within seam as well as between the LG-6 and LG-6A seams.

A “typical“ PGM spectrum for all Bushveld chromitites as proposed by *e.g.*, Junge et al. (2016) or Oberthür et al. (2016) is not supported by the results of the present study. Even though all included groups of the “typical” PGM were detected, different assemblages of different origin can be distinguished. This study thus extends the assemblages well-documented for the UG-2 (Kinloch 1982; Peyerl 1982; Penberthy and Merkle 1999; Voordouw et al. 2010) to the LG chromitites. Our results may be thus of general applicability, not only for the Thaba mine but also wider parts of the chromitites of the Bushveld Complex, taking the similarities between, *e.g.*, the general mineralogy, mineral chemistry, geology, host rocks within the Bushveld into account.

Acknowledgements

This is a contribution of the German/South African R&D project AMREP—Applied Mineralogy for Resource Efficiency of Platinum-Group Metals—funded by the German Ministry of Education and Research (BMBF; grant number BMBF 033R119E). We thank the Cronimet Mining Group for providing access to their core shed and drill core intersections from the Thaba mine and for the contribution of additional analytical data as well as information on the local geology and beneficiation. Andreas Bartzsch and Roland Würkert are thanked for sample preparation and Dr. Joachim Krause with his help at the EPMA. The comments of Thomas Oberthür to a previous version of this manuscript are gratefully acknowledged.

References

Aitchison, J (1986) The Statistical Analysis of Compositional Data. Monographs on Statistics and Applied Probability. Chapman & Hall Ltd., London (UK). (Reprinted in 2003 with additional material by The Blackburn Press).

Bachmann K, Frenzel M, Krause J, Gutzmer, J (2017). Advanced Identification and Quantification of In-Bearing Minerals by Scanning Electron Microscope-Based Image Analysis. Microscopy and Microanalysis 23(3):527-537. doi: 10.1017/S1431927617000460

Barnes S-J, Maier W (2002) Platinum-group element distributions in the Rustenburg Layered Suite of the Bushveld Complex, South Africa. In: Cabri LJ (editor) The geology, geochemistry, mineralogy and mineral beneficiation of platinum-group elements. Canadian Institute of Min Metall Pet Spec 54:431–458

Becker M, Brough C, Reid D, Smith D, Bradshaw D (2008) Geometallurgical characterisation of the Merensky Reef at Northam platinum mine–comparison of Normal, Pothole and Transitional reef types. In Ninth International Congress for Applied Mineralogy, Australasian Institute for Mining and Metallurgy:391–399

Becker M, Yorath G, Ndlovu B, Harris M, Deglon D, Franzidis J-P (2013) A rheological investigation of the behavior of two Southern African platinum ores. Minerals Engineering 49:92–97

Becker M, Wiese J, Ramonotsi, M (2014) Investigation into the mineralogy and flotation performance of oxidised PGM ore. Minerals Engineering 65: 24–32

Brough CP, Bradshaw DJ, Becker M (2010) A comparison of the flotation behaviour and the effect of copper activation on three reef types from the Merensky reef at Northam. Minerals Engineering 23(11):846–854

Bulatovic S (2003) Evaluation of alternative reagent schemes for the flotation of platinum group minerals from various ores. Minerals Engineering 16(10):931–939

Bushell, C (2012) The PGM flotation predictor: Predicting PGM ore flotation performance using results from automated mineralogy systems. Minerals Engineering 36:75–80

Cawthorn RG (1999) Platinum-group element mineralization in the Bushveld Complex—a critical reassessment of geochemical models. South African Journal of Geology 102:268–281

Cawthorn RG (2011) Geological investigations of the PGE distribution in the Bushveld Merensky and UG-2 chromite reefs. Journal South African Institute of Mining and Metallurgy 111:67–79

Chayes, F (1960) On correlation between variables of constant sum. Journal of Geophysical Research 65(12):4185–4193

Chetty D, Gryffenberg L, Lekgetho TB, Molebale IJ (2009) Automated SEM study of PGM distribution across a UG-2 flotation concentrate bank: implications for understanding PGM floatability. Journal of the Southern African Institute of Mining and Metallurgy 109(10):587–593

DERA (2013) Rohstoffwirtschaftlicher Steckbrief für Chrom/Chromit. Deutsche Rohstoffagentur in der BGR (DERA), 7pp

Dunn JG, Howes VL (1996) The oxidation of violarite. Thermochimica Acta, 282:305–316

Eales HV, Teigler B, Maier WD (1993) Cryptic variations of minor elements Al, Cr, Ti and Mn in Lower and Critical Zone orthopyroxenes of the western Bushveld complex. Mineralogical Magazine 57:257–264

Fahrmeir L, Hammerle A (1984) Multivariate Statistische Verfahren. Walter de Gruijter, Berlin:796p

Fandrich R, Gu Y, Burrows D, Moeller K (2007) Modern SEM-based mineral liberation analysis. International Journal of Mineral Processing 84:310–320.

Fisher, NI, Lewis T, Embleton BJ (1987) Statistical analysis of spherical data. Cambridge university press.

Fourie GP (1959) The chromite deposits in the Rustenburg area. South Africa Geological Survey Bulletin 27:45

Fraley C, Raftery AE (2002) Model-based Clustering, Discriminant Analysis and Density Estimation Journal of the American Statistical Association 97:611–631

Fraley C, Raftery AE, Murphy TB, Scrucca L (2012) mclust Version 4 for R: Normal Mixture Modeling for Model-Based Clustering, Classification, and Density Estimation. Technical Report No. 597, Department of Statistics, University of Washington

Gain SB (1985) The geologic setting of the platiniferous UG-2 chromitite layer on the farm Maandagshoek, eastern Bushveld Complex. Economic Geology 80:925–943

Gervilla F, Leblanc M, Torres-Ruiz J, Hach-Ali PF (1996) Immiscibility between arsenide and sulfide melts; a mechanism for concentration of noble metals. Canadian Mineralogist 34(3):485–502

Gu Y (2003) Automated scanning electron microscope based mineral liberation analysis. Journal of Minerals and Materials Characterization and Engineering 2:33–41

Hall AL (1932) The Bushveld igneous complex of the central transvaal. The Government Printer, Pretoria, 560 pp

Hiemstra SA (1985) The distribution of some platinum-group elements in the UG-2 chromitite layer of the Bushveld Complex. Economic Geology 80:944–957

Hiemstra SA (1986) The distribution of chalcophile and platinum-group elements in the UG-2 chromitite layer of the Bushveld complex. Economic Geology 81:1080–1086

Junge M, Oberthür T, Melcher F (2014) Cryptic variation of chromite chemistry, platinum group-element and -mineral distribution in the UG-2 chromitite—an example from the Karee Mine, western Bushveld Complex, South Africa. Economic Geology 109:795–810

Junge M, Wirth R, Oberthür T, Melcher F, Schreiber A (2015) Mineralogical siting of platinum group elements in pentlandite from the Bushveld Complex, South Africa. Mineralium Deposita 50:41–54

Junge M, Oberthür T, Osbahr I, Gutter P (2016) Platinum-group elements and minerals in the lower and middle group chromitites of the western Bushveld Complex, South Africa. Mineralium Deposita 51(7):841-852

Kinloch ED (1982) Regional trends in the platinum-group mineralogy of the critical zone of the Bushveld Complex, South Africa. Economic Geology 77:1328–1347

Lee CA (1996) A review of mineralization in the Bushveld complex and some other layered intrusions. In: Cawthorn RG (ed) Layered intrusions. Elsevier, Amsterdam, 103–145

Lee CA, Parry SJ (1988) Platinum-group element geochemistry of the lower and middle group chromitites of the eastern Bushveld Complex. Economic Geology 83:1127–1139

Li C, Ripley EM, Merino E, Maier W (2004) Replacement of base metal sulfides by actinolite, epidote, calcite and magnetite in the UG-2 and Merensky Reef of the Bushveld Complex, South Africa. Economic Geology 99:173–184

Maier WD, Barnes S-J (1999) Platinum-group elements in silicate rocks of the Lower, Critical, and Main zones at Union Section, western Bushveld Complex. Journal of Petrology 40:1647–1671

Maier WD, Barnes S-J (2008) Platinum-group elements in the UG-1 and UG-2 chromitites, and the Bastard reef, at Impala platinum mine, western Bushveld Complex. South Africa: Evidence for late magmatic cumulate instability and reef constitution: South African Journal of Geology 111:159–176

McLaren CH, De Villiers JPR (1982) The platinum-group chemistry and mineralogy of the UG-2 chromitite layer of the Bushveld Complex. Economic Geology 77:1348–1366

Naldrett A, Lehmann J (1988) Spinel non-stoichiometry as the explanation for Ni-, Cu, and PGE-enriched sulphides in chromitites. In: Prichard HM (ed) Geo-platinum 87, Elsevier Science Publ Ltd, 93–103

Naldrett A, von Gruenewaldt G (1989) Association of platinum-group elements with chromitite in layered intrusions and Ophiolite Complexes. Economic Geology 84:180–187

Naldrett AJ, Wilson A, Kinnaird J, Chunnett G. (2009a) PGE tenor and metal ratios within and below the Merensky Reef, Bushveld Complex: implications for its genesis. Journal of Petrology, 50(4):625–659. doi: 10.1093/petrology/egp015

Naldrett AJ, Kinnaird J, Wilson A, Yudovskaya M, McQuade S, Chunnett G, Stanley C (2009b) Chromite composition and PGE content of Bushveld chromitites: part 1—the lower and middle groups. Trans Inst Min Metall B 118:131–161

Naldrett AJ, Wilson A, Kinnaird J, Yudovskaya M, Chunnett G (2012). The origin of chromites and related PGE mineralization in the Bushveld Complex: new mineralogical and petrological constraints. Mineralium Deposita 47:209–232

Ndlovu B, Forbes E, Farrokhpay S, Becker M, Bradshaw D, Deglon D (2014) A preliminary rheological classification of phyllosilicate group minerals. Minerals Engineering 55:190-200

Oberthür T, Junge M, Rudashevsky N, de Meyer E, Gutter P (2016) Platinum-group minerals in the LG and MG chromitites of the eastern Bushveld Complex, South Africa. Mineralium Deposita 51:71–87. doi:10.1007/s00126-015-0593-0

Osbahr, I., Klemd, R., Oberthür, T., Brätz, H., and Schouwstra, R., 2013, Platinum-group element distribution in base-metal sulfides of the Merensky Reef from the eastern and western Bushveld Complex, South Africa: Mineralium Deposita 48:211–232

Osbahr I, Oberthür T, Klemd R, Josties A (2014) Platinum-group element distribution in base metal sulfides of the UG-2, Bushveld Complex, South Africa—a reconnaissance study. Mineralium Deposita 49:655–665

Osbahr I, Krause J, Bachmann K, Gutzmer J (2015) Efficient and Accurate Identification of Platinum-Group Minerals by a Combination of Mineral Liberation and Electron Probe Microanalysis with a New Approach to the Offline Overlap Correction of Platinum-Group Element Concentrations. Microscopy and Microanalysis 21(05):1080–1095. doi:10.1017/S1431927615000719

Penberthy CJ, Oosthuyzen EJ, Merkle RKW (2000) The recovery of platinum-group elements from the UG-2 chromitite, Bushveld Complex–a mineralogical perspective. Mineralogy and Petrology 68(1-3): 213–222

Penberthy CJ, Merkle RKW (1999) Lateral variations in the platinumgroup element content and mineralogy of the UG-2 chromitite layer, Bushveld Complex. South African Journal of Geology 102:240–250

Peyerl W (1982) The influence of the Driekop dunite pipe on the platinum-group element mineralogy of the UG-2 chromitite in its vicinity. Economic Geology 77:1432–1438

R Core Team (2016) R: A language and environment for statistical computing. R Foundation for Statistical Computing, Vienna, Austria. URL https://www.R-project.org/

Scoon RN, Teigler B (1994) Platinum-group element mineralization in the Critical zone of the Western Bushveld Complex: I. Sulfide-poor chromitites below the UG-2. Economic Geology 89:1094–1121

Shackleton NJ, Malysiak V, O'Connor CT (2007a) Surface characteristics and flotation behaviour of platinum and palladium arsenides. International Journal of Mineral Processing 85(1): 25–40

Shackleton NJ, Malysiak V, O’Connor CT (2007b) Surface characteristics and flotation behaviour of platinum and palladium tellurides. Minerals Engineering 20(13): 1232–1245

Smith AJB, Viljoen KS, Schouwstra R, Roberts J, Schalkwyk C, Gutzmer J (2013) Geological variations in the Merensky Reef at Bafokeng Rasimone Platinum Mine and its influence on flotation performance. Minerals Engineering 52: 155–168

Teigler B, Eales HV (1993) Correlation between chromite composition and PGE mineralization in the critical zone of the western Bushveld Complex. Mineralium Deposita 28:291–302

Tenailleau C, Pring A, Etschmann B, Brugger J, Grguric B, Putnis A (2006) Transformation of pentlandite to violarite under mild hydrothermal conditions. American Mineralogist 91(4): 706–709

Tolosana-Delgado, R (2012) Uses and misuses of compositional data in sedimentology. Sedimentary Geology 280: 60–79

Van den Boogaart KG, Tolosana R, Bren M (2014) compositions: Compositional Data Analysis. R package version 1.40-1. https://CRAN.R-project.org/package=compositions

Viljoen F, Knoper M, Rajesh H, Rose D, Greeff T (2012) Application of a field emission mineral liberation analyser to the in situ study of platinum-group element mineralisation in the Merensky Reef of the Bushveld Complex, South Africa. In Proceedings of the 10th International Congress for Applied Mineralogy (ICAM), Springer, Berlin, Heidelberg: 757–764

Von Gruenewaldt G (1977) The mineral resources of the Bushveld Complex. Minerals Science and Engineering 9(2):83–95

Von Gruenewaldt G, Hatton CJ, Merkle RKW, Gain SB (1986) Platinum-group element–chromite associations in the Bushveld Complex. Economic Geology 81:1067–1079

Voordouw RJ, Gutzmer J, Beukes, NJ (2010) Zoning of platinum group mineral assemblages in the UG-2 chromitite determined through in situ SEM-EDS-based image analysis. Mineralium Deposita 45:147–159. doi: 10.1007/s00126-009-0265-z

Wagner PA (1929) The platinum deposits and mines of South Africa. Oliver and Boyd, Edinburgh, 326pp

Xiao Z, Laplante AR (2004) Characterising and recovering the platinum group minerals—a review. Minerals Engineering 17: 961–979

Zeh A, Ovtcharova M, Wilson AH, Schaltegger U (2015) The Bushveld Complex was emplaced and cooled in less than one million years–results of zirconology, and geotectonic implications. Earth and Planetary Science Letters, 418, 103-114

Tables

Table 1 General information and available bulk chemical data of all investigated samples.

Borehole	Length	From	To	Cr_2O_3	FeO	SiO_2	MgO	Al_2O_3	CaO	P
LG-6	*in m*	*in m*	*in m*	*all data in wt%*						ppm
EL28	0.23	167.04	167.27	43.3	27.2	4.2	8.7	14.2	0.4	20
EL28D	**0.30**	**167.45**	**167.75**	**43.5**	**28.1**	**3.1**	**8.5**	**16.3**	**0.4**	**20**
ZK149	**0.83**	**94.68**	**95.51**	**43.2**	**25.0**	**5.0**	**9.2**	**14.0**	**0.3**	**20**
ZK149D	0.83	94.73	95.56	43.6	25.4	4.5	9.7	14.5	0.3	20
ZK144	**0.87**	**294.98**	**295.85**	**-**	**-**	**-**	**-**	**-**	**-**	**-**
ZK144D	0.93	294.89	295.82	44.0	26.9	3.5	8.7	13.6	0.3	20
LG-6A	*in m*	*in m*	*in m*	*all data in wt%*						ppm
EL32D	**0.19**	**252.59**	**252.78**	**-**	**-**	**-**	**-**	**-**	**-**	**-**
ZK136	0.20	268.95	269.15	44.7	25.7	4.1	11.3	14.6	0.4	28
ZK136D	**0.20**	**269.22**	**269.42**	**-**	**-**	**-**	**-**	**-**	**-**	**-**
SC42	**0.25**	**344.60**	**344.85**	**43.8**	**23.2**	**4.1**	**9.7**	**14.2**	**0.2**	**25**
SC42D	0.24	344.58	344.82	42.9	24.6	3.2	10.8	15.2	0.3	65

Please note that chromitite intersections in bold are considered in detail in this study. Boreholes marked with "D" are deflections of the motherhole and regarded as their most similar sample. Analyses were performed at Set Point Laboratories, Johannesburg. Cr_2O_3, FeO, SiO_2, MgO, Al_2O_3, CaO, P were analyzed by X-ray fluorescence (XRF). "-" = no geochemical analyses are available.

Table 2 Summary of MLA parameters.

SPL parameters		GXMAP parameters	
Voltage (kV)	25	Voltage (kV)	25
Probe current (nA)	10	Probe current (nA)	10
HFW (µm)	750	HFW (µm)	1000
BSE calib.	Au 252	BSE calib.	Au 250
Resolution (pixels)	1000 × 1000	Resolution (pixels)	500 × 500
Pixel size (µm/px)	0.75	Pixel size (µm/px)	2
Quartz EDX-count	2000	Quartz EDX-count	2000
BSE Range	100 - 255	GXMAP trigger	25
Frame Guide Size (px)	30	Step size (px)	8 × 8
Min. grain size (px)	2	Min. grain size (px)	4

SPL = sparse phase liberation measurement mode, HFW = horizontal field width, BSE = back scattered electrons, px = pixel, GXMAP = grain-based X-ray mapping measurement mode, EDX = energy dispersive X-ray spectroscopy

Table 3 Instrumental parameters applied to PGM/BMS analysis on the EPMA.

Element/ Line	Spectrometer/ Crystal	Peak position (mm)	Lower Backgr. (mm)	Upper Backgr. (mm)	Measurement Time Peak (s)	Measurement Time Backgr. (s)	12 kV Limit of Quantification* Sulfide/ PGM (ppm)	20 kV Limit of Quantification* Sulfide/ PGM (ppm)	Standards (ASTIMEX Standards Ltd.)
As Lα1,2	1 TAP	105.14	6.127	6.563	60	15	213/ 297	330/ 480	Arsenopyrite_AST
S Kα1	2 PETJ	171.599	5.061	-	40	20	117/ 170	157/ 177	Pentlandite_AST
Pd Lβ1	3 PETL	133.048	4.970	9.601	40	20	493/ 653	417/ 770	Palladium_AST
Rh Lα1,2	3 PETL	147.419	5.086	4.703	40	10	243/ 327	227/ 367	Rhodium_AST
Au Mα1	3 PETL	187.047	10.418	9.281	40	10	473/ 1023	603/ 817	Gold_AST
Pt Mα1	3 PETL	193.563	10.028	2.769	40	10	513/910	573/ 1050	Platinum_Ast
Ir Mα1	3 PETL	200.458	4.410	3.024	40	10	536/970	597/ 1040	Iridium_AST
Os Mα	3 PETL	207.728	4.093	3.127	40	10	543/ 880	597/ 940	Osmium_AST
Sb Lβ1	4 PETH	103.058	8.361	9.804	40	10	467/ 763	450/ 620	Stibnite_AST
Te Lα1	4 PETH	105.095	10.989	7.960	40	10	210/ 330	197/ 270	Tellurium_AST
Ru Lα1	4 PETH	155.161	3.218	-	40	20	133/ 210	143/203	Ruthenium_AST
Bi Mα1	4 PETH	163.863	12.114	13.374	40	10	337/ 550	430/ 560	BismuthSelenide_AST
Mo Lβ1	4 PETH	165.793	14.082	17.831	40	10	433/ 633	467/ 633	Molybdenum_AST
Cu Kα1	5 LIFH	107.259	1.960	2.131	40	10	867/ 1510	297/ 467	Copper_AST
Ni Kα1	5 LIFH	115.466	6.521	2.887	40	10	660/ 1130	257/ 427	Pentlandite_AST
Co Kα1	5 LIFH	124.555	3.106	2.745	40	10	473/ 787	240/ 343	Cobalt_AST
Fe Kα1	5 LIFH	134.797	5.100	3.000	40	10	383/ 633	197/ 313	Pentlandite_AST

All standards supplied by ASTIMEX Standards Ltd. Limit of Quantification = 10 × limit of detection.

Table 4 Representative EPMA analyses of major PGM. Z – numbers of atoms per formula unit. b.d.l. – below detection limit; apfu – atoms per formula unit.

No.	300	193	414	511	127	145	186	51	90	115	99	243	71	329	294	273	239
Comment	EL28D-3_080	EL28D-2_071	ZK136D-2_054	ZK136D-2_113	SC42-2_097	SC42-2_115	SC42-2_156	SC42-2_021	ZK149-5_063	ZK149-5_088	ZK149-5_072c	EL32D-4_049	ZK149-5_044c	EL32D-4_135	EL32D-4_131	EL32D-4_079	EL32D-4_045
Seam	LG-6	LG-6	LG-6A	LG-6A	LG-6A	LG-6A	LG-6A	LG-6A	LG-6	LG-6	LG-6	LG-6A	LG-6	LG-6A	LG-6A	LG-6A	LG-6A
Mineral	Cooperite	Cooperite	Braggite	Vysotskite	Vysotskite	Vysotskite	Malanite	Laurite	Laurite	Laurite	Platarsite	Platarsite	Hollingworthite	Hollingworthite	Sperrylite	Geversite	Stibiopalladinite
all data in wt%																	
As	bdl	bdl	bdl	bdl	bdl	bdl	bdl	bdl	bdl	bdl	27.64	29.08	35.02	30.14	35.11	0.6	bdl
S	15.37	14.98	18.8	22.71	23.65	24.91	26.29	38.57	38	36.69	11.75	13.14	10.91	15.99	0.34	0.09	0.24
Pd	0.43	0.59	26.46	32.71	46.6	63.25	0.1	bdl	bdl	0.06	bdl	0.03	bdl	bdl	3.26	bdl	66.9
Rh	bdl	bdl	bdl	bdl	bdl	bdl	10.57	0.68	0.24	0.9	4.03	16.3	24.88	44.95	0.06	bdl	bdl
Au	bdl	bdl	bdl	bdl	bdl	bdl	bdl	bdl	bdl	bdl	bdl	bdl	bdl	bdl	bdl	bdl	0.14
Pt	80.27	80.18	53.24	34.9	16.49	0.38	38.77	bdl	bdl	bdl	35.45	22.07	24.06	0.36	48.59	42.33	0.06
Ir	bdl	bdl	bdl	bdl	bdl	bdl	8.28	2.65	2.8	4.91	1.72	2.52	bdl	1.65	bdl	bdl	0.03
Os	0.1	0.05	bdl	bdl	bdl	bdl	0.5	1.72	6.68	8.8	2.02	5.56	0.32	0.24	0.03	0.06	bdl
Sb	bdl	bdl	bdl	bdl	bdl	bdl	bdl	bdl	bdl	bdl	bdl	0.43	bdl	3.77	4.45	47.52	30.42
Te	bdl	bdl	bdl	bdl	bdl	bdl	bdl	bdl	bdl	bdl	bdl	bdl	bdl	bdl	0.02	0.25	bdl
Ru	bdl	bdl	bdl	bdl	bdl	bdl	0.07	55.3	52.55	47.42	14.89	8.28	3.24	2.35	bdl	0.01	bdl
Bi	bdl	bdl	bdl	bdl	bdl	bdl	bdl	bdl	bdl	bdl	bdl	bdl	bdl	bdl	5.12	7.96	bdl
Mo	bdl	bdl	bdl	bdl	bdl	bdl	1.2	0.15	0.15	0.12	bdl	bdl	bdl	bdl	bdl	bdl	bdl
Cu	0.04	0.04	0.08	0.1	0.18	bdl	12.06	0.02	bdl	bdl	bdl	bdl	bdl	bdl	bdl	0.01	bdl
Ni	2.39	1.77	2.46	10.55	11.01	10.81	0.4	0.07	0.03	0.14	0.14	0.4	0.21	0.1	0.19	0.04	0.27
Co	0.03	0.02	bdl	0.02	bdl	bdl	1.48	bdl	bdl	bdl	bdl	0.07	0.02	0.02	0.06	bdl	0.05
Fe	1.89	2.05	1.11	1.37	1.34	1.05	1.42	1.18	0.73	1.37	1.34	0.52	0.28	0.7	0.43	0.68	0.69
Total	100.52	99.67	102.15	102.37	99.26	100.41	101.14	100.35	101.18	100.41	98.98	98.37	98.92	100.26	97.66	99.55	98.79
all data is given as apfu																	
As	-	-	-	-	-	-	-	-	-	-	0.963	0.959	1.154	0.851	1.688	0.036	-
S	0.987	0.982	1.002	1.011	1	0.986	4.018	2	2.006	1.993	0.956	1.012	0.84	1.055	0.038	0.012	0.058
Pd	0.008	0.012	0.425	0.439	0.594	0.754	0.004	-	-	0.001	-	0.001	-	-	0.11	-	4.863
Rh	-	-	-	-	-	-	0.503	0.011	0.004	0.015	0.102	0.391	0.597	0.924	0.002	-	-
Au	-	-	-	-	-	-	-	-	-	-	-	-	-	-	-	-	0.006
Pt	0.847	0.864	0.466	0.255	0.115	0.002	0.974	-	-	-	0.474	0.279	0.304	0.004	0.897	0.969	0.002
Ir	-	-	-	-	-	-	0.211	0.023	0.025	0.045	0.023	0.032	-	0.018	-	-	0.001
Os	0.001	0.001	-	-	-	-	0.013	0.015	0.059	0.081	0.028	0.072	0.004	0.003	0.001	0.001	-
Sb	-	-	-	-	-	-	-	-	-	-	-	0.009	-	0.066	0.132	1.743	1.933
Te	-	-	-	-	-	-	-	-	-	-	-	-	-	-	0.001	0.009	-
Ru	-	-	-	-	-	-	0.003	0.91	0.88	0.817	0.384	0.202	0.079	0.049	-	0.001	-
Bi	-	-	-	-	-	-	-	-	-	-	-	-	-	-	0.088	0.17	-
Mo	-	-	-	-	-	-	0.061	0.003	0.003	0.002	-	-	-	-	-	-	-
Cu	0.001	0.001	0.002	0.002	0.004	-	0.93	0.001	-	-	-	-	-	-	-	0.001	-
Ni	0.084	0.063	0.071	0.257	0.254	0.234	0.033	0.002	0.001	0.004	0.006	0.017	0.009	0.004	0.012	0.003	0.035
Co	0.001	0.001	-	0.001	-	-	0.123	-	-	-	-	0.003	0.001	0.001	0.004	-	0.006
Fe	0.07	0.077	0.034	0.035	0.033	0.024	0.125	0.035	0.022	0.043	0.063	0.023	0.012	0.027	0.028	0.055	0.095
Z	2	2	2	2	2	2	7	3	3	3	3	3	3	3	3	3	7

Table 5 Representative compositions of major sulfide minerals (BMS) as analyzed by EPMA.

Mineral		S	Cu	Fe	Co	Ni	Pb
(1) Chalcopyrite	Median	34.62	32.91	30.28	bdl	0.02	bdl
	Range	33.77-37.19	31.71-33.27	29.63-32.05	bdl	bdl-0.20	bdl
(2) Pyrite	Median	53.32	0.02	45.01	0.61	0.33	bdl
	Range	49.21-55.17	bdl-0.37	41.34-46.52	bdl-1.49	0.01-3.46	bdl
(3) Pentlandite	Median	33.22	bdl	27.68	0.91	37.57	bdl
	Range	30.14-41.19	bdl-0.15	19.12-31.71	0.08-1.14	32.95-40.62	bdl
(4) Co-Pentlandite	Median	33.52	bdl	28.86	4.46	32.67	bdl
	Range	30.90-35.57	bdl	21.03-30.86	3.40-5.29	27.89-35.31	bdl
(5) Millerite	Median	35.73	bdl	2.56	bdl	61.39	bdl
	Range	35.13-37.78	bdl	2.17-4.59	bdl-0.80	57.86-62.18	bdl
(6) Violarite	Median	42.84	0.08	29.30	0.29	23.82	bdl
	Range	41-32-44.29	bdl-0.15	27.66-30.91	0.25-0.33	23.31-27.26	bdl

Notes: (1): n=43; (2): n=44; (3): n=70; (4): n=35, pentlandite analyses with >2.00 wt% Co; (5): n=3; (6): n=4; b.d.l. – below detection limit.

Table 6 Grouping of PGM (left) and BMS (right), respectively.

PGM			BMS		
Group	Mineral	$Group_{Geostatistics}$	Group	Mineral	$Group_{Geostatistics}$
(PGE)AsS	hollingworthite, irarsite, platarsite, sperrylite	PGM(1)	Ccp	chalcopyrite	BMS(1)
(Pt,Pd)S	cooperite, braggite, vysotskite	PGM(2)	Co-Pn	Co-rich pentlandite	BMS(2)
$(Pt,Rh)_2CuS_4$	cuprorhodsite, malanite	PGM(3)	Mlr	millerite	BMS(3)
$(Ru, Ir, Os)S_2$	erlichmannite, laurite	PGM(4)	Pn	pentlandite	BMS(4)
Alloys(Fe,Sn)	native platinum, rustenburgite, tetraferroplatinum	PGM(5)	Py/Po	pyrite, pyrrhotite	BMS(5)
Alloys(Sb,Bi)	geversite, insizwaite, stibiopalladinite, sudburyite	PGM(6)	Vio	violarite	BMS(6)

Table 7 Modal mineralogy of investigated LG-6 and LG-6A drill core intersections. All values are presented as area%.

Mineral	ZK144-LG-6	EL28D-LG-6	ZK149-LG-6	EL32D-LG-6A	ZK136D-LG-6A	SC42-LG-6A
Alteration Silicates	5.7	0.9	3.1	11.8	2.2	0.4
Carbonates	<0.1	<0.1	<0.1	3.7	<0.1	<0.1
Chromite	83.3	89.9	93.5	66.8	68.2	75.2
Silicates	10.8	9.2	3.4	17.7	29.6	24.4
Others	0.2	<0.1	<0.1	<0.1	<0.1	<0.1
Total	100.0	100.0	100.0	100.0	100.0	100.0

Table 8 Summary of important parameters of determined assemblages for mineral beneficiation.

<table>
<tr><th>Assemblage</th><th>PGM species</th><th>BMS species</th><th colspan="2">Mineral association/ Gangue mineralogy</th><th>PGM grain sizes</th><th>BMS particle sizes</th></tr>
<tr><td>(I)</td><td rowspan="2">PGM-(Cu)-sulfides; alloys of Fe, Sn</td><td rowspan="2">Pn + Ccp + Py + Mlr</td><td colspan="2">BMS, Chromite, Silicate</td><td rowspan="3">min: <1μm, max: 20μm, avg: 4-5μm</td><td rowspan="3">max: 300μm, avg: >30μm</td></tr>
<tr><td>(II)</td><td rowspan="2">alteration silicates</td><td>silicates</td></tr>
<tr><td>(III)</td><td>PGM-(sulf)arsenides; alloy of Sb, Bi</td><td>(Co-rich) Pn ± Ccp ± Py</td><td>carbonates, chromite</td></tr>
</table>

Figures

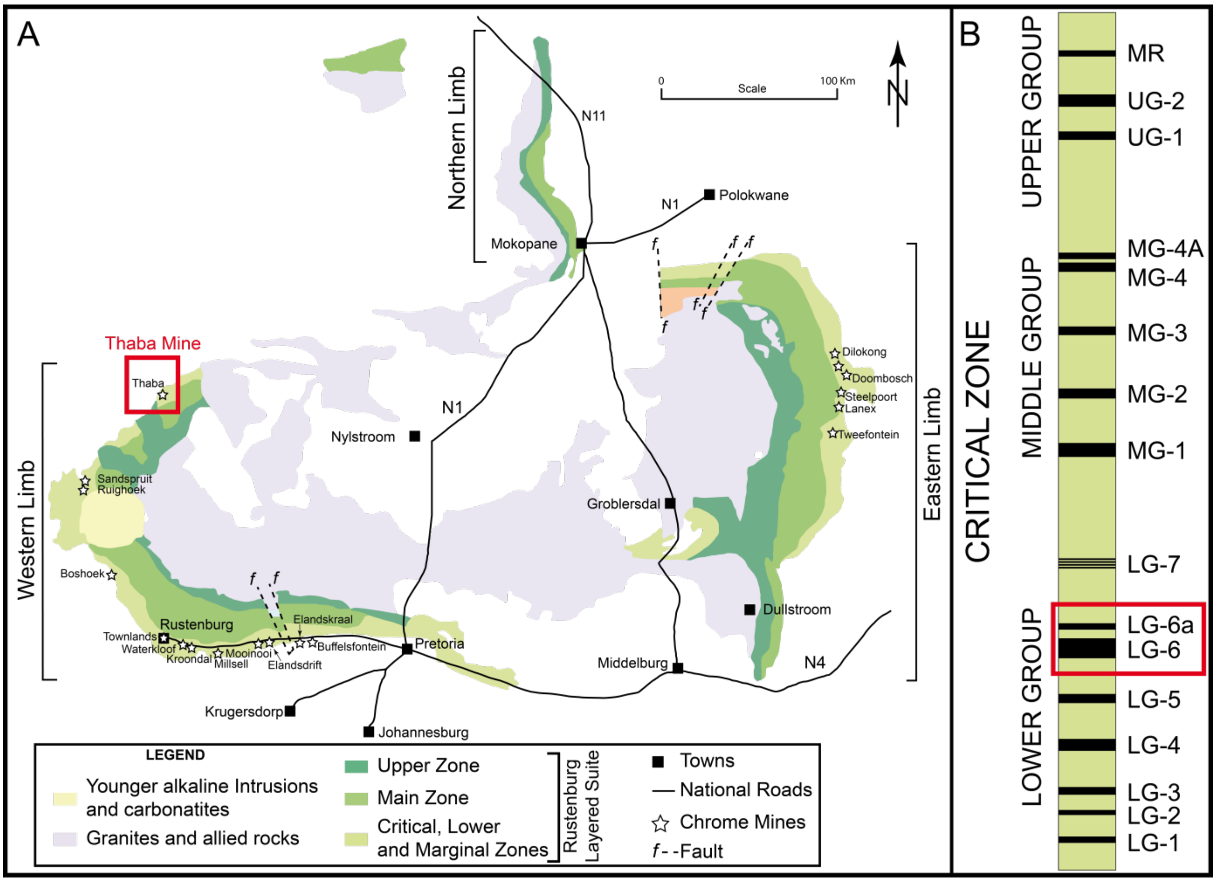

Figure 1(A) Geological map of the Bushveld Complex. The location of the Thaba mine is marked in red. (B) Stratigraphic column of the Critical Zone showing the positions of the major chromitite seams and of the Merensky Reef (MR) (modified from Oberthür et al. 2016).

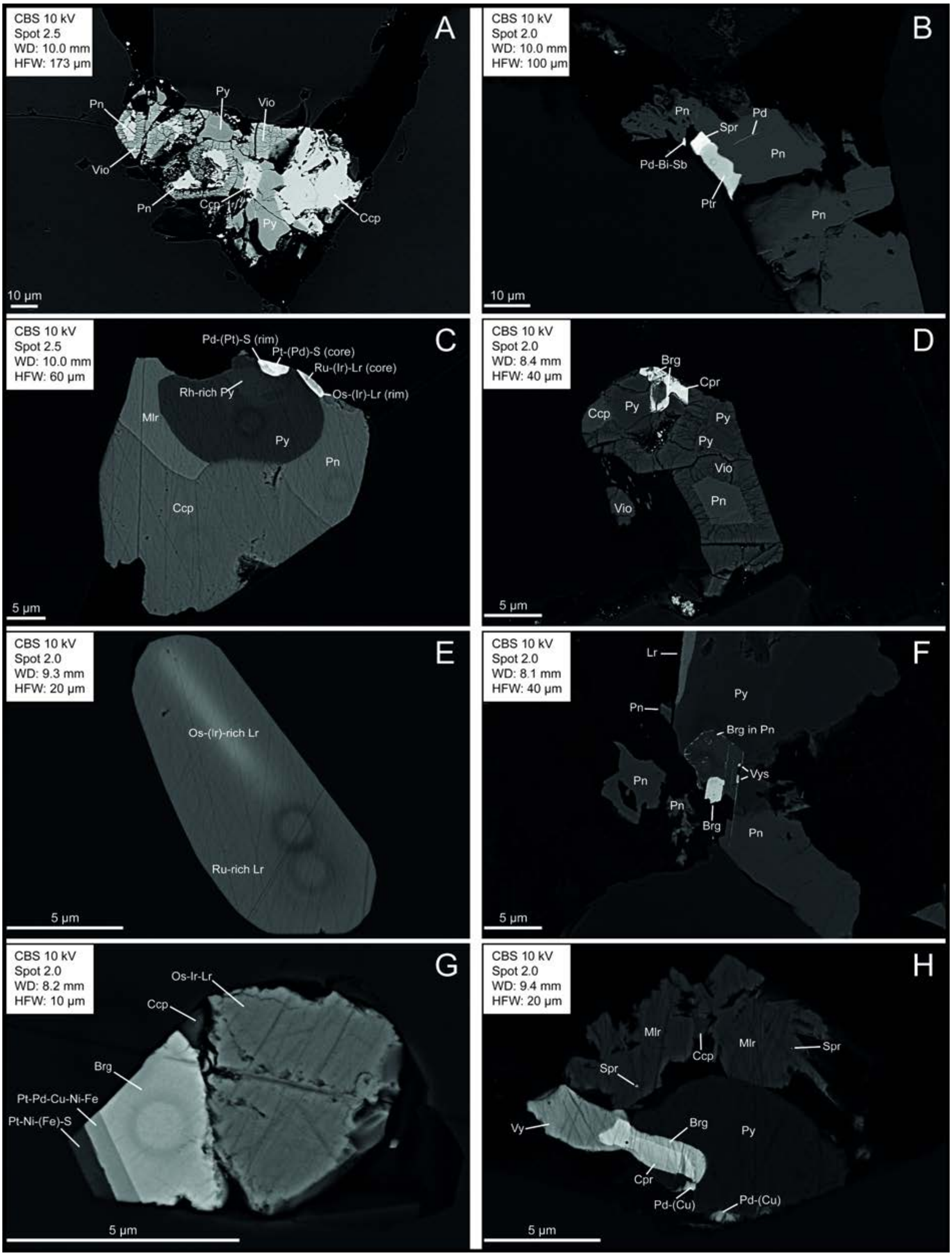

Figure 2 Back-scattered electron (BSE) images of sulfides and PGM in polished sections of the LG-6 and LG-6A chromitite seams. Scale bar and SEM conditions are displayed in the images. (A) Sulfide aggregate containing pyrite (Py), chalcopyrite (Ccp), pentlandite (Pn) and violarite (Vio) in intersection EL28D-LG-6. Please note the alteration of pentlandite into violarite. (B) Platarsite (Plr), Sperrylite (Spr) and a PdBiSb alloy intergrown with Pn in intersection ZK149-LG-6. Please note the Pd dominated lamellae in Pn. (C) Sulfide droplet interstitial to chromite containing millerite (Mlr), Py, Pn and Ccp in intersection SC42-LG-6A. Note the segregation of PPGE and IPGE into different discrete PGM (Braggite (Brg) and Laurite (Lr), respectively) as well as the exsolution of Rh into pyrite (slightly brighter). Both grains show further segregation of Pt and Ru, respectively, located in the core and Pd and Os in the rim. (D) Sulfide aggregate intergrown with a PPGE mineral showing different Braggite

(Brg) – Cooperite (Cpr) compositions in intersection EL28D-LG-6. Note the alteration of Pn into Vio. (E) Laurite grain as an inclusion in chromite in intersection SC42-LG-6A. Note the brighter area due to a higher concentration of Os and Ir. (F) Brg intergrown with sulfides in intersection ZK136D-LG-6A. Note the exsolution of Pt-Pd into the surrounding sulfides during cooling – keeping the original shape of the Brg grain and the formation of Vysotskite (Vys). (G) PGE particle composed of various PGM, both, sulfides (Brg and Lr) as well as alloys as inclusion in chromite in intersection ZK136D-LG-6A. (H) Pt-Pd sulfide of various composition ranging from Vys to Cpr intergrown with various sulfides in intersection SC42-LG-6A. Note the nanoinclusions of Spr in Mlr and a Pd-Cu rich bright phase.

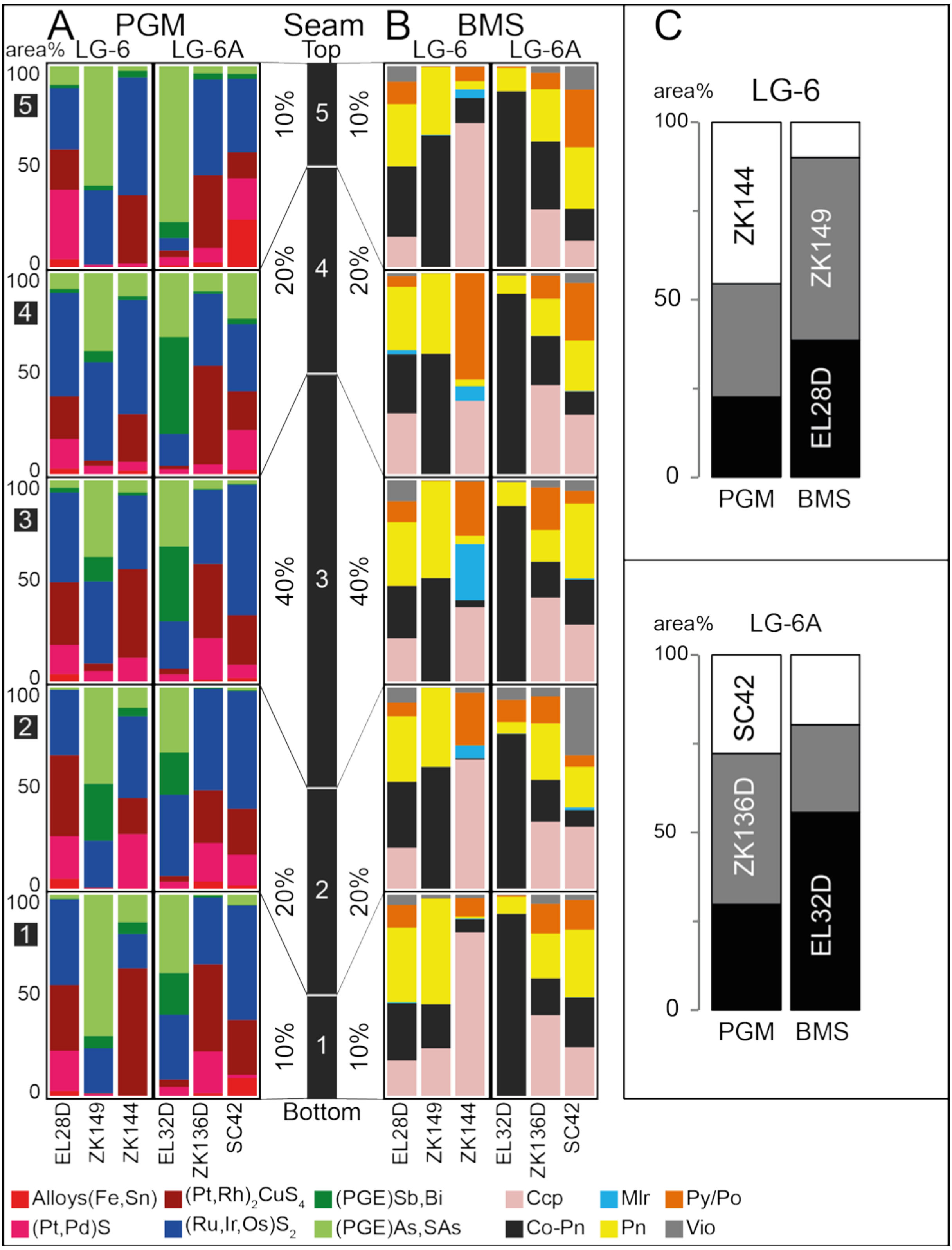

Figure 3 Comparison of MLA thin sections data for drill cores of the LG-6 and LG-6A seam intersections. Thirty samples were analyzed for each seam. (A, B) 100% stacked histograms that show the PGM (for detailed grouping see text) (A) and sulfide (B) assemblages of LG-6 and LG-6A intersections from bottom to top (sectors 1 to 5). (C) Based on normalized thin sections, PGM and BMS area within the sample (μm^2) were summed for each drill core separately. The relative distribution of PGM and BMS (area%) in seam LG-6 and LG-6A, respectively, is shown in stacked bar plots. "Seam" displays the division into five sampled distinct sectors (sectors 1-5, from bottom to top) and each sector was sampled randomly to prepare an individual polished thin section for study. For details see text.

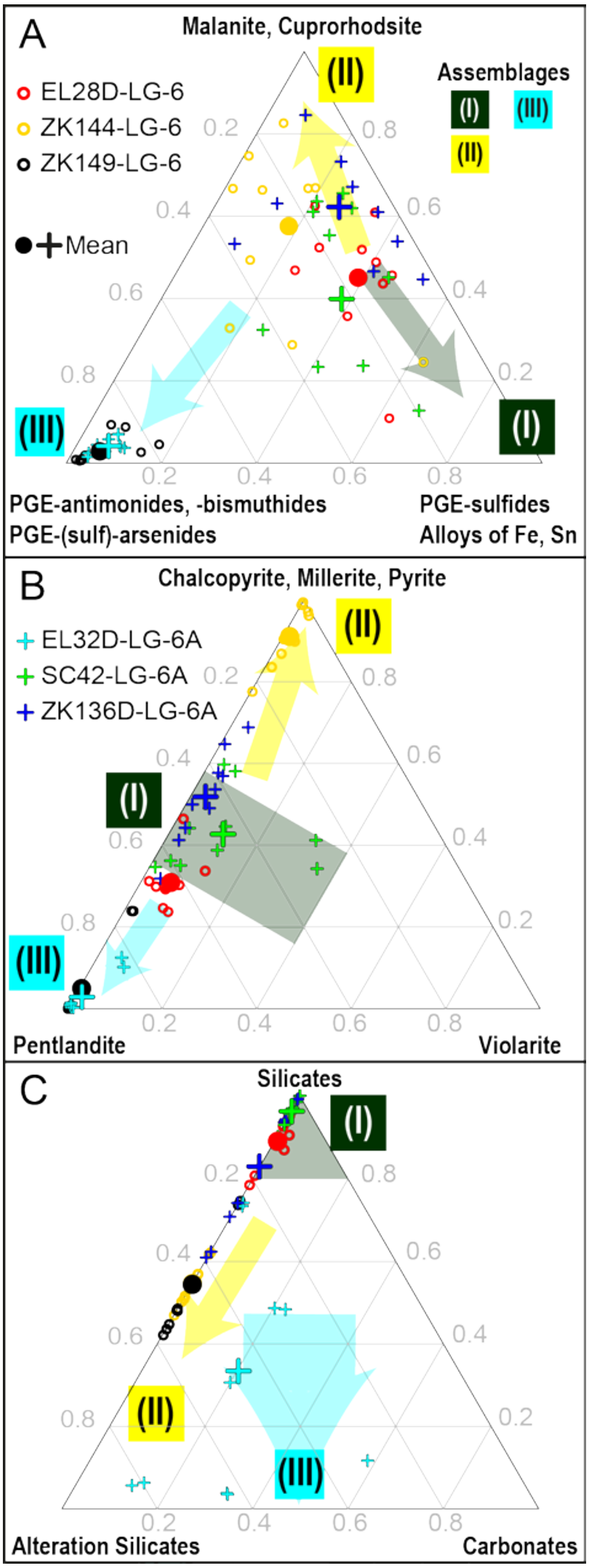

Figure 4 Modal proportions of all thin sections (and the corresponding means) of LG-6 and LG-6A samples for (A) PGM, (B) BMS, and (C) Gangue mineral groups projected in a ternary diagram.

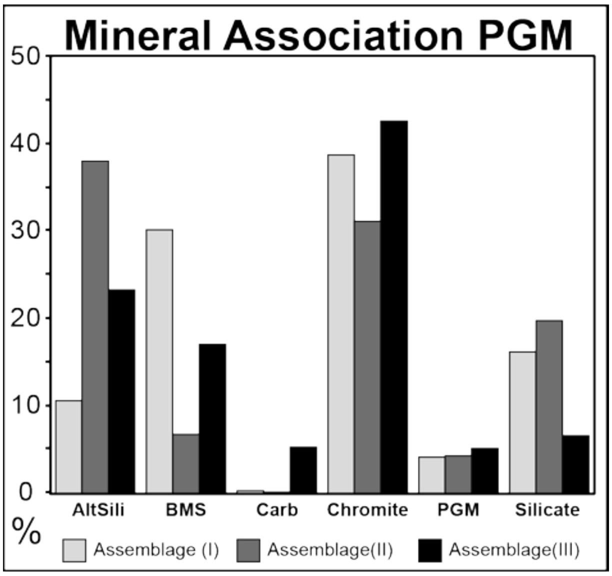

Figure 5 Histogram of mineral association of PGM comparing assemblages (I), (II), (III). Assemblage (I) displays high abundances of PGM-sulfides and alloys of Fe and Sn, while assemblage (II) is dominated by PGM-Cu-sulfides. Assemblage (III), on the other hand, comprises high amounts of PGM-sulfarsenides and PGM-arsenides together with PGE-antimonides, -bismuthides and scant –bismuthotellurides.

Appendix A

Methods – Reproducibility of MLA data

Quantification of the reproducibility and statistical significance of the analyses was performed through (1) analyzing a thin section twice in the same analytical run (in-run duplication), and (2) by re-polishing of the sample to analyze a second surface of the same sample. Results are displayed in Figure A1. In-run analysis displays a relative standard deviation (2σ) for total area%^{PGM} of 5 % for sample ZK149-LG-6 and 4 % for sample ZK136D-LG-6A, while total area%^{BMS} and wt%^{Modal} show 2σ values below 2 % and 0.5 % for both samples, respectively. The combined in-run duplicates of surface A with surface B, 2SDs are 32 % in sample ZK149 and 15 % in sample ZK136D-LG-6A for total area%^{PGM}, while total area%^{BMS} and total area%^{Gangue} show 2σ values below 2 % and 3 % for both samples, respectively.

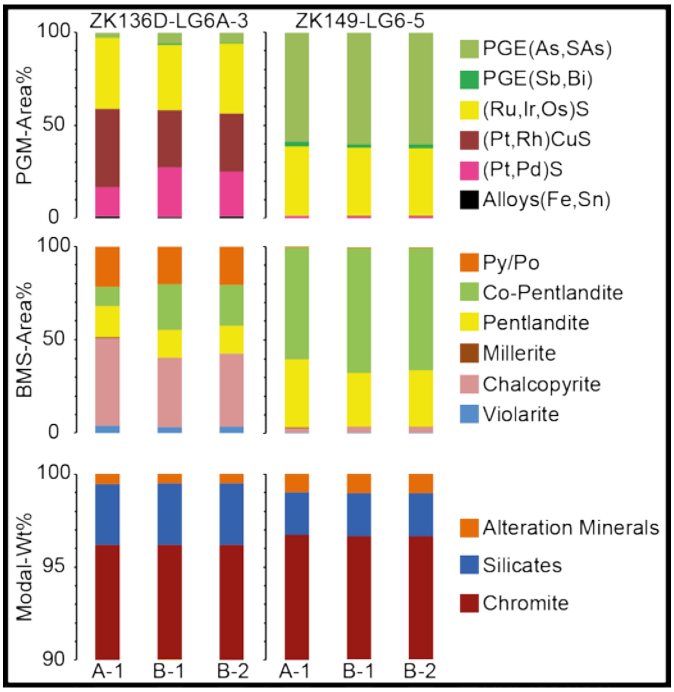

Figure A1 Stacked histograms showing the proportions of PGM species (in terms of area%^{PGM}), base metal sulfides (in terms of area%^{BMS}), and the modal mineralogy in wt% for samples ZK136D-LG-6A-3 and ZK149-LG-6-5. A-1: surface A; B-1: surface B-1; B-2: in-run duplicate of surface B-1.

Methods - Electron probe microanalysis (EPMA)

Quantitative analyses were also performed for amphibole, chromite, clinopyroxene, feldspar, olivine, orthopyroxene, serpentine and talc. Concentrations of Na, Mg, Al (all TAP); Si, K, Ca (all PETJ); Cr, V, Ti (all PETL); Zn, Ni, Co, Fe, Mn (all LIFH) were measured using K_{α} – lines. Certified reference materials provided by ASTIMEX Standards Ltd. were used for calibration. An electron beam diameter of 5 µm was set at 20kV/ 12 nA and the ZAF approach was used for matrix correction (atomic number–absorption–fluorescence; Philibert, 1963; Reed, 1965; Philibert & Tixier, 1968). Dwell times were set to 15s (Na), 20s (Si, Cr, Ni), and 30s (K, Ca, Fe, Mn), 40s (Mg, Al, V, Ti, Zn, Co). Offline overlap corrections were performed for Zn $L_{\beta 1}$ on Na $K_{\alpha 1,2}$; Mn $K_{\alpha 1}$, Ti $K_{\alpha 1}$, Cr $K_{\beta 1,3}$ on Al $K_{\alpha 1,2}$; Ni $K_{\alpha 1}$ on Ca $K_{\alpha 1}$; V $K_{\beta 1,3}$ on Cr $K_{\alpha 1}$; Ti $K_{\beta 1,3}$ on V $K_{\alpha 1}$; Mn $K_{\beta 1,3}$ on Fe $K_{\alpha 1}$; and Cr $K_{\beta 1,3}$ on Mn $K_{\alpha 1}$ as explained in Osbahr et al. (2015).

Finally, EPMA results were used to generate mineral standard spectra with a known composition for MLA measurements. Therefore, mineral standards were taken close to EPMA measurements. This approach allows a detailed differentiation of silicates, such as different feldspar compositions, amphiboles, pyroxenes and alteration silicates.

Results - Geochemistry

5PGE+Au (Pt,Pd,Rh,Ir,Ru,Au) contents are around 1 ppm for LG-6 samples and 1.5 ppm for the LG-6A. In general, the total sulfur content ranges between 100 – 200 ppm (<250 ppm), except intersection ZK144-LG-6, which contains only around 70 ppm. Detailed information are provided with the electronic supplementary material.

Figure A2 displays detailed geochemical assays of two selected drill core intersections of the LG-6 (ZK149-LG-6 and ZK144-LG-6). The profiles display a rather stable Cr_2O_3 content around 43-51 wt%. Slight fluctuations, especially in ZK149-LG-6 display massive chromitite intercalated with ~1 cm pyroxene-rich bands or pyroxene oikocrysts. 5PGE+Au contents are 900 ppb and 950 ppb with a Pt/Pd ratio around 2.2 and 4 and Pt/Ru ratios around 0.9 for intersections ZK144-LG-6 and ZK149-LG-

6, respectively. Both profiles display 5PGE+Au profiles with a "M-shape"; ZK144-LG-6 displays a smooth variation in the overall PGE contents, ranging from ~700 ppb to 1100 ppb, while ZK149-LG-6 displays spikes with minimum single element contents of roughly 370 ppb and a maximum of 1600 ppb. The Ni+Cu plot displays different patterns, however, with variable contents for both of the examples. Cu/ (Cu+Ni) ratios are 0.02 and 0.01 for ZK144-LG-6 and ZK149, respectively. In general, the LG-6 is sulfur poor, with contents ranging from 70 ppm (ZK144-LG-6) to 130 ppm (ZK149-LG-6), on average.

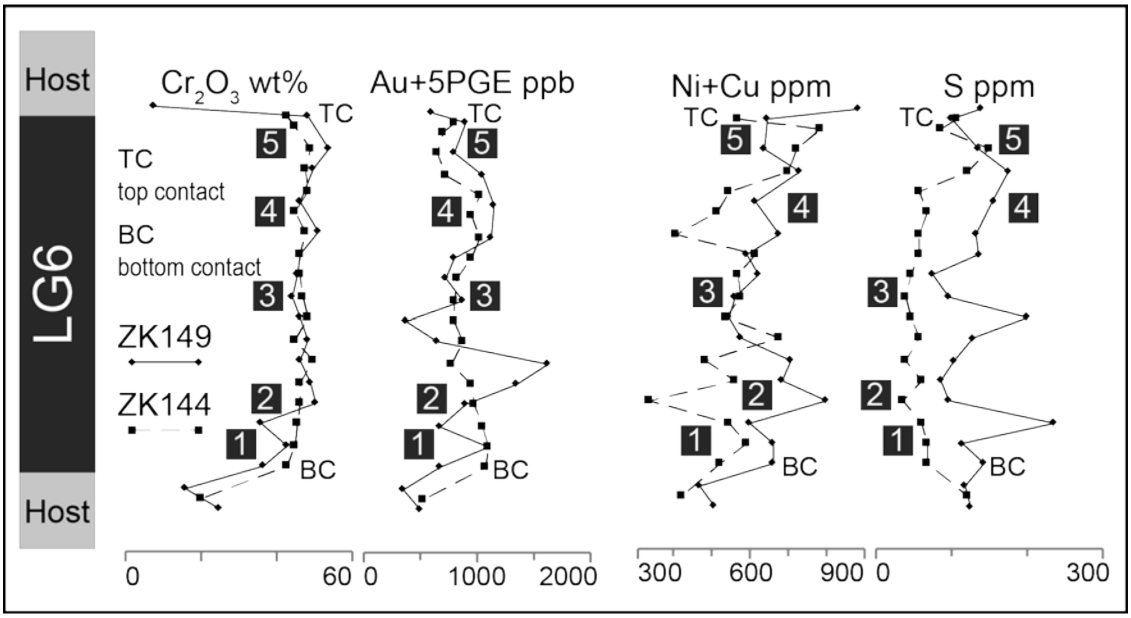

Figure A2 Detailed geochemistry of Cr_2O_3, Au+PGE (6E), Ni+Cu, and S concentrations versus stratigraphic height, normalized to 100 (ZK149: 83 cm; ZK144: 93 cm) in the LG6. Note the bottom (BC) and top contact (TC) of the intersections. 6E analyzed by Ni fire assay, aqua-regia digestion and ICP-MS finish, sulfur analyzed by "LECO" combustion.

Results - EPMA analyses – silicate minerals and chromite

Altogether, 359 analyses on LG-6A samples were obtained to describe the mineral chemistry of various silicate minerals as well as chromite in the LG seams. Table A1displays representative analyses of this sample set, extended by some analyses of important mineral compositions, namely Al-rich chromite, olivine, and serpentine, contained in a MG sample set due to a lack of these minerals in the measured LG sections. Mineral standard spectra for further MLA analysis were taken on grains with a known composition for a better identification during quantitative mineralogical assessment.

Figure A3A displays two different types of pyroxenes. One type yields an orthopyroxene X_{En}=78-85, X_{Fs} = 13-19 and X_{Wo} = 0.5-9 and is hereafter referred to as enstatite. The second type shows a slight trend from augitic to mainly diopsidic compositions and is composed of X_{En}=45-52, X_{Fs} = 5-9 and X_{Wo} = 38-48 (hereafter referred to as diopside). Amphiboles can be best described as magnesio-hornblende. Feldspars shown in Figure A3B yield plagioclase compositions ranging from andesine to bytownite, however, also minor albite and anorthite were analyzed by EDX measurement. Furthermore, sanidine with X_{Or} up to 90 % was encountered. For both, pyroxene and feldspar, there were no significant differences between samples detected. Chromite was analyzed in sample EL32D_LG-6A and ZK136D_LG-6A (Figure A3C). Data might indicate differences between samples, as sample EL32D_LG-6A displays low Fe^{3+} and slightly higher Al contents than ZK136D_LG-6A.

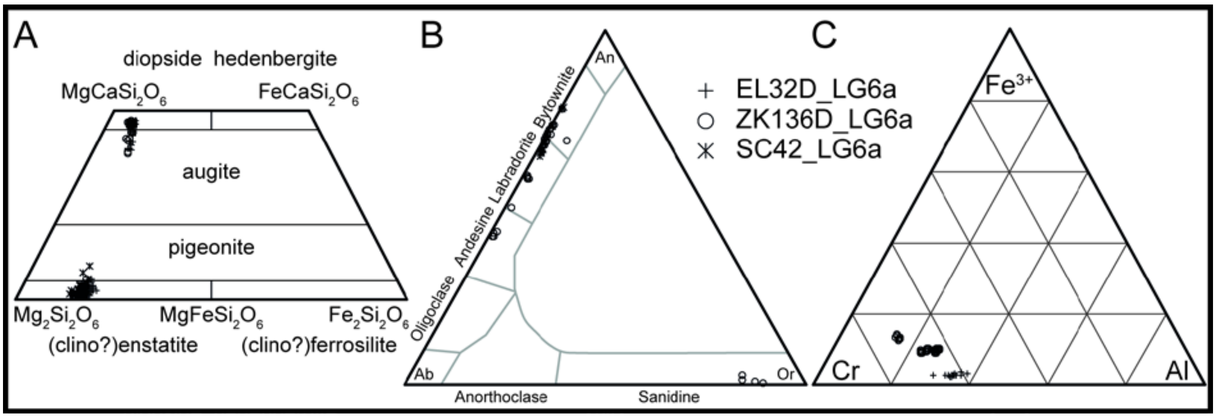

Figure A3 Ternary plots of EPMA measurements. (A) Classification diagram of pyroxene after Morimoto (1988). Both types of pyroxene – enstatite (orthopyroxene) and (augite)-diopside are rather chemically homogeneous. (B) Classification diagram of feldspar with endmembers anorthite (*An*), albite (*Ab*), alkalifeldspar/ orthoclase (*Or*). Beside plagioclase with variable composition alkali feldspar with sanidine composition was detected. (C) Ternary plot of trivalent cations, Cr, Al and Fe^{3+} in chromite. Note that the data show only little variation, however, all analyses of intersection EL32D_LG-6A display a lower concentration in Fe^{3+} compensated by a higher Al content.

Table A1 Representative EPMA analyses of all relevant silicate minerals and chromite, used for the MLA Mineral Reference List.

No.	346	330	23	207	221	120	228	391	197	445	192	166	132
Core	ZK136D	EL32	EL32D	EL32D	SC42	ZK146	SC42	ZK136D	EL32D	EL32	EL32D	EL32D	ZK146
Seam	LG-6A	MG1	LG-6A	LG-6A	LG-6A	MG1	LG-6A	LG-6A	LG-6A	MG1	LG-6A	LG-6A	MG1
Mineral	Chromite	Al-Chromite	Chromite	ClinoPx	OrthoPx	Olivine	Plagioclase	K-Feldspar	Muscovite	Biotite	Amphibole	Talc	Serpentine
all data in wt%													
Na_2O	bdl	bdl	bdl	0.35	0.01	0.02	2.36	1.19	0.11	0.26	1.84	0.05	0.02
MgO	4.84	14.26	6.56	18.00	31.44	45.36	0.04	0.01	0.54	18.84	16.64	25.69	35.97
Al_2O_3	7.43	48.11	17.40	2.00	1.38	0.00	32.54	18.33	34.88	20.71	10.25	0.38	0.01
SiO_2	0.04	0.72	0.03	53.28	55.32	40.03	49.18	63.29	47.30	39.39	47.60	59.28	40.58
K_2O	bdl	bdl	bdl	bdl	0.01	0.00	0.04	15.44	9.66	9.24	0.15	0.02	0.03
CaO	bdl	bdl	bdl	19.44	0.74	0.03	15.64	0.10	0.26	1.52	11.70	0.20	0.03
Cr_2O_3	50.81	14.86	46.53	0.99	0.56	0.00	0.23	bdl	0.02	0.06	2.01	0.09	0.01
V_2O_3	0.46	0.34	0.44	0.05	0.03	0.00	0.01	0.02	0.02	0.01	0.11	0.01	0.01
TiO_2	0.47	0.05	0.84	0.22	0.09	0.00	bdl	0.04	bdl	0.27	1.30	0.02	0.02
ZnO	0.13	0.76	0.11	bdl	bdl	bdl	bdl	bdl	bdl	bdl	bdl	bdl	bdl
NiO	0.12	0.13	0.14	0.04	0.08	0.29	bdl	0.04	bdl	0.11	0.12	0.05	0.32
CoO	0.13	0.13	0.09	0.02	0.03	0.03	bdl	bdl	0.01	0.02	0.02	0.01	0.03
MnO	0.32	0.09	0.30	0.16	0.24	0.20	bdl	bdl	0.01	0.02	0.08	0.04	0.05
FeO	25.33	16.88	24.52	5.40	9.88	13.92	0.28	0.35	2.24	4.82	5.91	8.69	7.59
Fe_2O_3	9.35	1.60	1.87										
Total	99.42	97.92	98.82	99.97	99.82	99.89	100.31	98.81	95.05	95.27	97.72	94.54	84.68
all data is given as apfu													
Na				0.025	0.001	0.001	0.208	0.108	0.015	0.035	0.198	0.014	
Na (A)											0.315		
Mg	2.019	4.763	2.591	0.979	1.653	1.693	0.003	0.001	0.053	1.981	3.565	5.096	5.302
Al	3.678	19.052	8.152	0.086	0.058		1.748	1.014	2.731	1.722	1.735	0.060	0.002
Al IV				0.055	0.049				0.857	1.221	1.160	0.060	
Al VI				0.031	0.008				1.874	0.502	0.576		0.002
Si	0.024	0.323	0.014	1.945	1.951	1.002	2.241	2.969	3.143	2.779	6.840	7.889	4.012
Si (T1)											2.840		
K							0.003	0.924	0.819	0.831	0.027	0.004	0.004
Ca				0.760	0.028	0.001	0.763	0.005	0.018	0.115	1.802	0.028	0.004
Cr	16.873	3.948	14.627	0.029	0.016		0.008	0.000	0.001	0.004	0.229	0.010	0.001
V	0.160	0.095	0.146	0.002	0.001			0.001	0.001	0.001	0.014	0.001	0.001
Ti	0.199	0.016	0.333	0.006	0.002			0.001		0.014	0.140	0.002	0.001
Zn	0.026	0.126	0.022										
Ni	0.026	0.024	0.029	0.001	0.002	0.006		0.002		0.006	0.014	0.005	0.025
Co	0.029	0.022	0.019	0.001	0.001	0.001			0.001	0.001	0.003	0.001	0.002
Mn	0.076	0.017	0.068	0.005	0.007	0.004			0.001	0.001	0.009	0.004	0.004
Fe^{2+}	5.928	3.163	5.433	0.165	0.291	0.292	0.011	0.014	0.124	0.284	0.710	0.967	0.628
Fe^{3+}	2.955	0.404	0.560										
Vac											0.658		
Total	31.993	31.952	31.995	4.003	4.010	3.000	4.985	5.038	6.907	7.776	15.600	14.082	9.985
Cr/Al	4.587	0.207	1.794										
Mg#	0.254	0.601	0.323	0.86	0.85								
FFE	0.333	0.113	0.093										
Cr#	0.821	0.172	0.642										
Cr/Fe	1.33	0.71	1.56										
Sum IV				2.000	2.000								
Sum VI				2.003	2.010								
X_{Wo}				39.92	1.43								
X_{En}				51.43	83.81								
X_{Fs}				8.65	14.77								
Fo						85.10							
An							78.35	0.50					
Or							0.26	89.08					
X_{Mg}									0.053	0.637	0.834		
Na+K(A)											0.342		

Please note the analyses for Al-chromite, olivine, biotite and serpentine were taken from a different sample set of MG1 samples from the same locality. Calculation of chromite is normalized to 32 O; pyroxene is normalized to 6 O; olivine is normalized to 4 O; feldspar is normalized to 8 O; mica is normalized to 11 O; amphibole is normalized to 23 O; talc is normalized to 22 O; and serpentine is normalized to 14 O. apfu – atoms per formula unit.

ANOVA

An ANOVA was performed – followed by standard F-tests – to investigate the variability of the samples and to determine assemblages for classification according to the sub-compositions area%^{PGM}, area%^{BMS} and area%^{Gangue} (see legend in Figure A4A). Variability of the samples was tested for four explanatory factors (“surfaces A/B”, “intra seam”, “inter core” and “inter seam” (see in the methods section for definition of these explanatory factors). “Surfaces A/B” compares the results obtained for the two different polished surfaces (A and B) analysed for each sample. This explanatory factor is found to have no significant influence on the tested ANOVA model, which allows the conclusion that the exact position of the sample surface examined by MLA has no significant effect on the results obtained. Most notably, it suggests that the “nugget effect” (small scale variability) is negligible.

The explanatory factor “intra seam” considers the variance between samples of a different stratigraphic position within a sampled seam, *i.e.* if seams have systematically different mineral assemblages within their respective confines. The factor “intra seam” does have a significant influence for the variance of both, area%^{PGM} and area%^{BMS} and a highly significant influence for the variance of area%^{Gangue}. The two factors “inter seam” (considering systematic differences between the two studied seams, LG-6 and LG-6A) and “inter core” (considering systematic differences between different drill core intersections) show close interrelation, meaning that variance induced by “inter seam” will be a part of the variance induced by “inter core”. While the F-tests for the factor “inter seam” are non-significant for area%^{PGM} and area%^{BMS}, and highly significant for area%^{Gangue}, the factor “inter core” yields highly significant results in all cases. This suggests that systematic differences between distinct seams intersected within the same drill core are of minor importance compared to differences encountered between drill cores from different sites on the mine lease area.

Figure 4A shows the variance distribution for the two most relevant factors. “Inter core” is by far the most important explanatory factor, explaining between 59 and 77 % of the total variance. In comparison, the factor “intra core” explains only 6 % of total variance – a value that is similar for all sub-compositions. As mentioned above, the factor “seam” was not considered further, as it explains only between 2 and 13 % of the “inter core” variance for area%^{PGM} and area%^{BMS} and area%^{Gangue}. The factor “residuals” reports the variance that cannot be assigned to any of the previously mentioned factors and ranges between 23 and 35 % of the total variance. A detailed evaluation of the explanatory factor “inter core” for all sub-compositions based on ratios of certain mineral groups is shown in Figure A4B. The chosen ratios explain the bulk total variance, *i.e.* reflect the distribution of the group members. According to the ANOVA model the main part of the total variance in area%^{PGM} is invested in predicting the ratios [PGE -sulfarsenides and PGE-antimonides, -bismuthides vs. PGE –sulfides, -Cu-sulfides and -alloys of Fe,Sn]; *i.e.* these groups show a strong negative correlation and form distinctly different mineral assemblages. Furthermore, the ratio [PGE-Cu-sulfides vs. PGE –sulfides and –alloys of Fe,Sn] explains a significant portion of the total variance, and may be used to distinguish two more PGM mineral assemblages. The variability of IPGE -sulfides is rather low and only marginally explained by the factor “inter core”. The area%^{BMS} “inter core” variance is mostly related to the variability of (Co-rich) pentlandite with respect to the geometric average of the other four BMS considered (chalcopyrite, millerite, pyrite and violarite). The ratios [chalcopyrite vs. millerite] and [chalcopyrite and millerite vs. violarite] do also have relevant contributions. The mentioned relationships correspond well to the area%^{PGM} distribution, *i.e.* PGE-sulfarsenide/ -alloy of Sb,Bi-rich assemblages represent the same set of samples as the (Co-rich) pentlandite dominated BMS assemblages (forming assemblage (III)). On the other hand, PGE-(Cu)–sulfides and -alloys of Fe,Sn occur together with rather chalcopyrite, millerite, pyrite, violarite dominated samples – resulting in assemblage (I) and (II). The latter assemblages can be further subdivided into PGE-Cu-sulfides + chalcopyrite and millerite-rich samples (assemblage (II)), in contrast to assemblage (I) where a PGE-sulfide-rich assemblage is associated with a rather variable BMS assemblage consisting of chalcopyrite, pentlandite, pyrite and variable amounts of violarite.

In the area%^{Gangue} sub-composition total "inter core" variance is best described using the ratios [alteration silicates and silicates vs. carbonate] followed by [alteration silicates vs. silicates]. While carbonate-rich samples are associated with PGM-BMS assemblage (III), silicate-rich samples dominate PGM-BMS assemblage (I). Significant amounts of alteration silicates may occur in samples belonging to PGM-BMS assemblages (II) and (III).

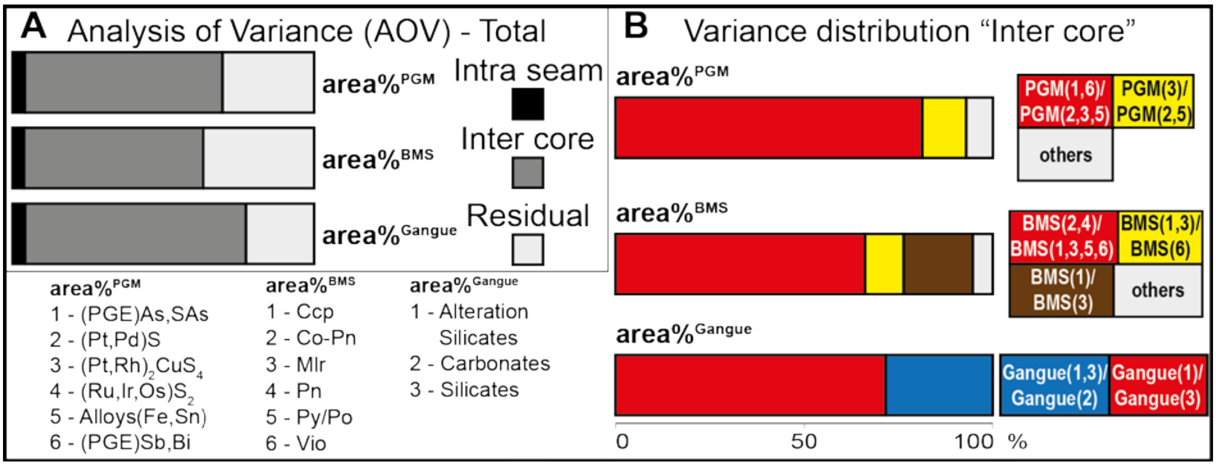

Figure A4 Stacked histograms of the results of an analysis of variance (AOV) of the modal mineralogy for PGM, BMS and rock forming minerals (Others). (A) Total variance distribution for area%^{PGM}, area%^{BMS} and area%^{Gangue}. (B) Variance distribution based on defined ratios of certain PGM/BMS/Gangue groups. For simplification, further reference to any group members will be as following, e.g. (PGE)As,AsS = PGM(1); Alloys(Sb,Bi) = PGM(6); Ccp = BMS(1), etc. (cf. Table 6; legend in (A)).

Cluster analysis

For a quantitative assessment of the variability of the mineral association a cluster analysis was performed according to the sub-compositions of PGM (without IPGE sulfides) and BMS. The results were linked to the mineral assemblages defined in the previous chapter (*ANOVA*).

Despite the very low total abundance of BMS (< 0.02 area% in all samples), PGM show a strong preferred association with BMS; they also show a close association with alteration silicates, occurring both in interstitial positions and as inclusion. PGM are only to a much lesser extent associated with silicates and chromite. PGM occur predominantly interstitial to chromite (with minor inclusions cf. Figure 2G). BMS show a very similar association to PGM.

The cluster analysis results in three distinct clusters: a dominant and two minor, for both PGM [$n_{Cluster1}$ = 5, $n_{Cluster2}$ = 16, $n_{Cluster3}$ = 39] and for BMS [$n_{Cluster1}$ = 39, $n_{Cluster2}$ = 12, $n_{Cluster3}$ = 9] (Figure A5). PGM cluster 1 consists of samples with a high silicate and lower chromite content, where most PGM occur in association with BMS. Cluster 2 includes carbonate-rich samples and PGM associated with alteration silicates and carbonates. Cluster 3, on the other hand, represents high chromite, high alteration silicate and low silicate content samples; PGM in this cluster are intergrown with alteration silicates and silicates. BMS cluster 1 is marked by high silicate/ alteration silicate ratios, where BMS occur predominantly as polymineralic aggregates intergrown with both alteration silicates and silicates. In contrast, the BMS cluster 3 lacks BMS aggregates and and includes samples with low silicate/alteration silicate ratios. BMS are closely associated with silicates and alteration silicates in these samples. Similar to PGM cluster 2, the BMS cluster 2 represents carbonate-rich samples. Both, PGM and BMS mineral associations thus define similar clusters - implying a separation of silicate-dominated from alteration silicate and/or carbonate-dominated clusters. BMS and PGM tend to be associated with alteration minerals, if present, hence, establishing cluster 1 as typical for assemblage (I) seems valid. Furthermore, cluster 2 can be assigned to assemblage (III), while cluster 3 mainly represents the alteration silicate-rich members of assemblage (II) and (III).

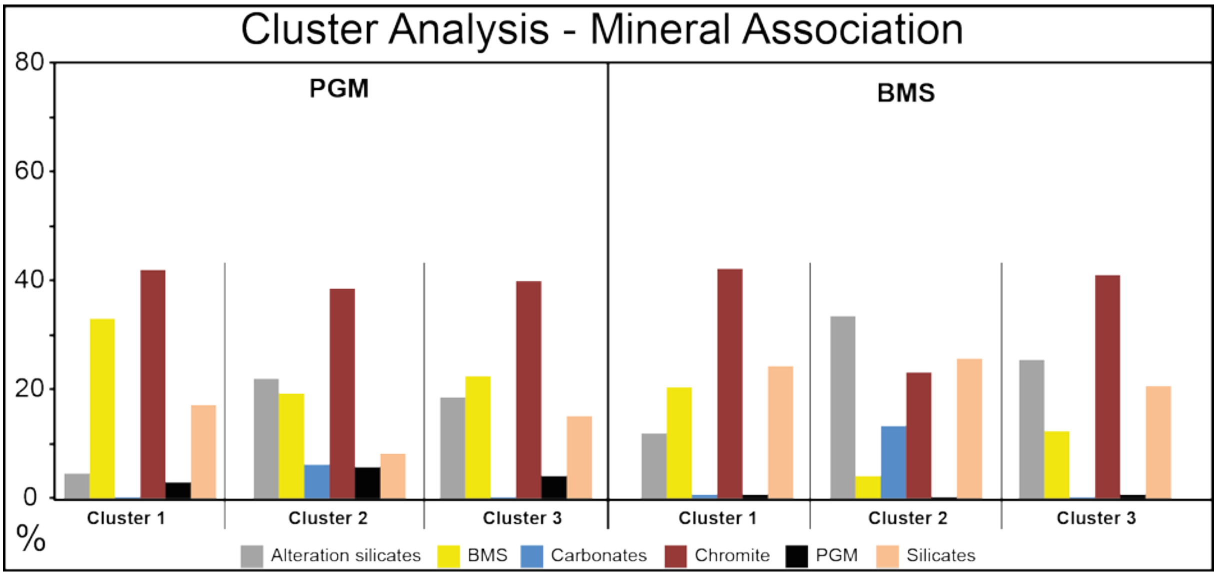

Figure A5 Histograms of average mineral associations of clusters defined by two cluster analysis for sub-compositions PGM (without IPGE –sulfides) and BMS, respectively. Color codes are explained below corresponding histograms. Cluster (I) displays high abundances of PGM-sulfides and alloys of Fe and Sn together with BMS dominated by pentlandite + chalcopyrite + pyrite. Cluster (II) comprises high amounts of PGM-sulfarsenides and PGM-arsenides together with PGE-antimonides, -bismuthides and scant –bismuthotellurides. Corresponding BMS are strongly dominated by pentlandite and Co-rich pentlandite. On the one hand, cluster (III) represents samples dominated by PGM-Cu-sulfide corresponding with high amounts of chalcopyrite. On the other hand, a minor amount of samples contains significant portions of PGM-sulfarsenides, -arsenides, -antimonides, and -bismuthides corresponding with a high abundance of pentlandite.

References

Morimoto N (1988) Nomenclature of pyroxenes. Mineralogy and Petrology 39(1):55–76

Philibert J (1963) X-ray optics and x-ray microanalysis. In Proceedings of the Third International Symposium, Stanford University, Pattee H.H., Cosslett, V.E. & Engström, A. (Eds.), New York, NY: Academic Press: 379

Philibert J, Tixier R (1968) Electron penetration and the atomic number correction in electron probe microanalysis. J Phys 1: 685–694

Reed SJB (1965) Characteristic fluorescence corrections in electron probe microanalysis. Br J Appl Phys 16: 913–926